Received: 30 August 2019 | Revised: 15 January 2020 | Accepted: 16 January 2020

DOI: 10.1111/bre.12437

ORIGINAL ARTICLE

Basin Research | IAS EAGE | WILEY

Distinct petrographic responses to basin reorganization across the Triassic–Jurassic boundary in the southwestern Barents Sea

Lina H. Line[1] | **Reidar Müller**[1] | **Tore G. Klausen**[3] | **Jens Jahren**[1] | **Helge Hellevang**[1,2]

[1]Department of Geosciences, University of Oslo, Oslo, Norway

[2]The University Centre in Svalbard (UNIS), Longyearbyen, Norway

[3]Petrolia NOCO AS, Bergen, Norway

Correspondence
Lina Hedvig Line, Department of Geosciences, University of Oslo, P.O. Box 1047, Blindern, 0316 Oslo, Norway.
Email: l.h.line@geo.uio.no

Funding information
VISTA, Grant/Award Number: 6270; OMV Norge

Abstract

A general shift towards higher mineralogical and textural maturity changes the reservoir character across the Triassic–Jurassic transition in the southwestern Barents Sea basin (SWBSB), largely affecting the hydrocarbon prospectivity in the region. Petrographic and geochronological provenance data presented in this paper suggest that the shift from mineralogically immature to mature sandstones initiated during the deposition of the Norian–Rhaetian Fruholmen Formation, and varies with basin location. Strong contrasts between the Fruholmen Formation and underlying formations are associated with proximity to the rejuvenated Caledonian and Fennoscandian hinterlands and are mainly restricted to the southern basin margins. In the basin interior, subtle petrographic variations between the Fruholmen Formation and older Triassic sandstones reflect a distal position relative to the southern hinterland. The long-lived misconception of a regional compositional contrast in the Arctic at the turn of the Norian can be attributed to higher sampling frequency associated with hydrocarbon exploration activity along the southern basin margins, and masking by increased annual precipitation and subsequent reworking during the Jurassic. Geothermal signatures and rearrangement of ferric clay material across the Carnian–Norian transition support a recycled origin for the Fruholmen Formation in the basin interior. As the closest tectonically active region at the time, the Novaya Zemlya fold-and-thrust belt represents the best provenance candidate for polycyclic components in Norian–Rhaetian strata. In addition to recycling in the hinterland during the Late Triassic, local erosion of exposed intrabasinal highs and platforms at the Triassic–Jurassic transition represents a second process where thermodynamically unstable mineral components originally sourced from the Uralides may be removed. Textural and mineralogical modification may also have occurred in marginal-marine depositional environments during periods with elevated sea level. Mature sediment supply from the rejuvenated hinterland in the south, multiple cycles of reworking and gradual accumulation of polycyclic grains have likely led to the extreme compositional maturity registered in the Tubåen, Nordmela and Stø formations in the

The peer review history for this article is available at https://publons.com/publon/10.1111/bre.12437.

SWBSB. It is likely that increased annual precipitation since the latest Carnian had an amplifying effect on sandstone maturation across the Triassic–Jurassic boundary, but we consider the effect to be inferior compared to provenance shifts and reworking. Findings from this study are important for understanding compositional and textural maturity enhancement processes in siliciclastic sedimentary basins.

KEYWORDS

Barents sea, Jurassic, petrography, provenance, Triassic

Highlights

- A shift from compositionally immature to mature sandstones initiated in the southwestern Barents Sea basin during deposition of the Norian-Rhaetian Fruholmen Formation.
- Compositional maturity of siliciclastic sandstones is linked to proximity to rejuvenated hinterlands, mainly restricted to southern basin margins.
- Geothermal and petrographic signatures support a recycled origin for the Fruholmen Formation in the basin interior.
- Novaya Zemlya represents the best provenance candidate for polycyclic components in Norian-Rhaetian strata.
- Sediment modification occurred through multiple stages of reworking and in marginal-marine environments.

1 | INTRODUCTION

Over a 30-million-year period, the southwestern Barents Sea basin (SWBSB) went from being dominated by high rates of sedimentation and accommodation in the Triassic to the development of regionally condensed sections characterized by low sedimentation rates and bypass in the Early-Middle Jurassic (Ryseth, 2014). Accompanying this major shift in basin configuration is an extensive mineralogical and textural maturation of sandstone packages that have been registered throughout the Greater Barents Sea (Fleming et al., 2016; Flowerdew et al., 2019; Mørk, 1999). Although most commercial hydrocarbon discoveries have been made in Upper Triassic to Middle Jurassic sandstones, few published studies target the mechanisms behind the increased reservoir quality across the Triassic–Jurassic (T–J) boundary in the SWBSB on a regional scale.

The majority of published petrographic studies from Upper Triassic and Jurassic successions in the SWBSB has been conducted in areas open to hydrocarbon exploration activity, which, until recently, has concentrated around the southern margins of the basin. In these areas, infill differences between the Triassic and Jurassic periods have been attributed to rejuvenation of the Fennoscandian and Caledonian hinterlands, increased annual precipitation and reduced subsidence rates (Ryseth, 2014). This change is associated with a dramatic increase in sediment maturity and is thoroughly documented across the Early Norian flooding surface along the southern basin margins (Bergan & Knarud, 1993; Fleming et al., 2016; Mørk, 1999). By contrast, the petrographic development in the offshore basin interior has largely been neglected in previous investigations targeting the Upper Triassic–Middle Jurassic succession. Fleming et al. (2016) recorded geochemical and compositional discrepancies between a petrographic dataset from the basin interior and data from the southern basin margin. The geographical differences were linked to extensive fluvial input from the rejuvenated Fennoscandian provenance along the southern basin margins, and widespread recycling of underlying Uralide-sourced sediments in the northern areas (Fleming et al., 2016). An Upper Triassic–Middle Jurassic petrography database also exists from Svalbard and the surrounding archipelagos at the northwestern edge of the shelf (Haile et al., 2018; Mørk, Knarud, & Worsley, 1982; Mørk, 1999) but spatial correlation with the SWBSB is challenging without substantial data control from the offshore basin interior.

For the first time, an extensive petrographic database is available for the Upper Triassic–Middle Jurassic succession in the offshore interior of the SWBSB. By comparing petrographic and provenance signatures from the basin interior to the southern basin margin, our results allow for a more nuanced interpretation of the Triassic–Jurassic transition than previously recorded in published literature. We investigate temporal changes in provenance and sediment supply at various locations in the SWBSB. Other sandstone maturation processes, such as climatic weathering and reworking, are also investigated. The development of the Norian–Rhaetian Fruholmen Formation is of particular interest as this stratigraphic unit constitutes half of the Triassic time interval and likely represents a transitional depositional sequence between the high-accommodation setting and the subsequent

low-accommodation basin configuration that became pronounced in the Jurassic. The findings from this study are relevant for all interested in basin-scale processes influencing sediment texture and composition, ultimately leading to improved reservoir quality.

2 | GEOLOGICAL BACKGROUND

The Barents Sea is presently a wide continental shelf bordered by two steep shear margins separating the Norwegian and Greenland seas from the Eurasian Basin in the north (Figure 1a). The present basin configuration is the result of several compressional phases related to orogenic events in the Precambrian–Cambrian (Timanian), Silurian–Devonian (Caledonian), latest Devonian–earliest Carboniferous (Ellesmerian–Svalbardian), Carboniferous–Permian (Uralian), Late Triassic (Taimyr, Pai Khoi and Novaya Zemlya) and Palaeogene (Spitsbergen–Eurekan; Faleide et al., 2018). In addition, two major extensional phases occurred during the Late Devonian to mid-Permian and in mid-Late Jurassic (Henriksen et al., 2011). Changing orientation of rift systems has resulted in a fan-shaped array of half-grabens and structural highs (Figure 1b) that appears to follow zones of crustal weakness inherited from the Caledonian orogeny 420–359 million years ago (Gudlaugsson, Faleide, Johansen, & Breivik, 1998). Each extensional event was followed by post-rift subsidence, facilitating deposition of carbonate, evaporite and siliciclastic

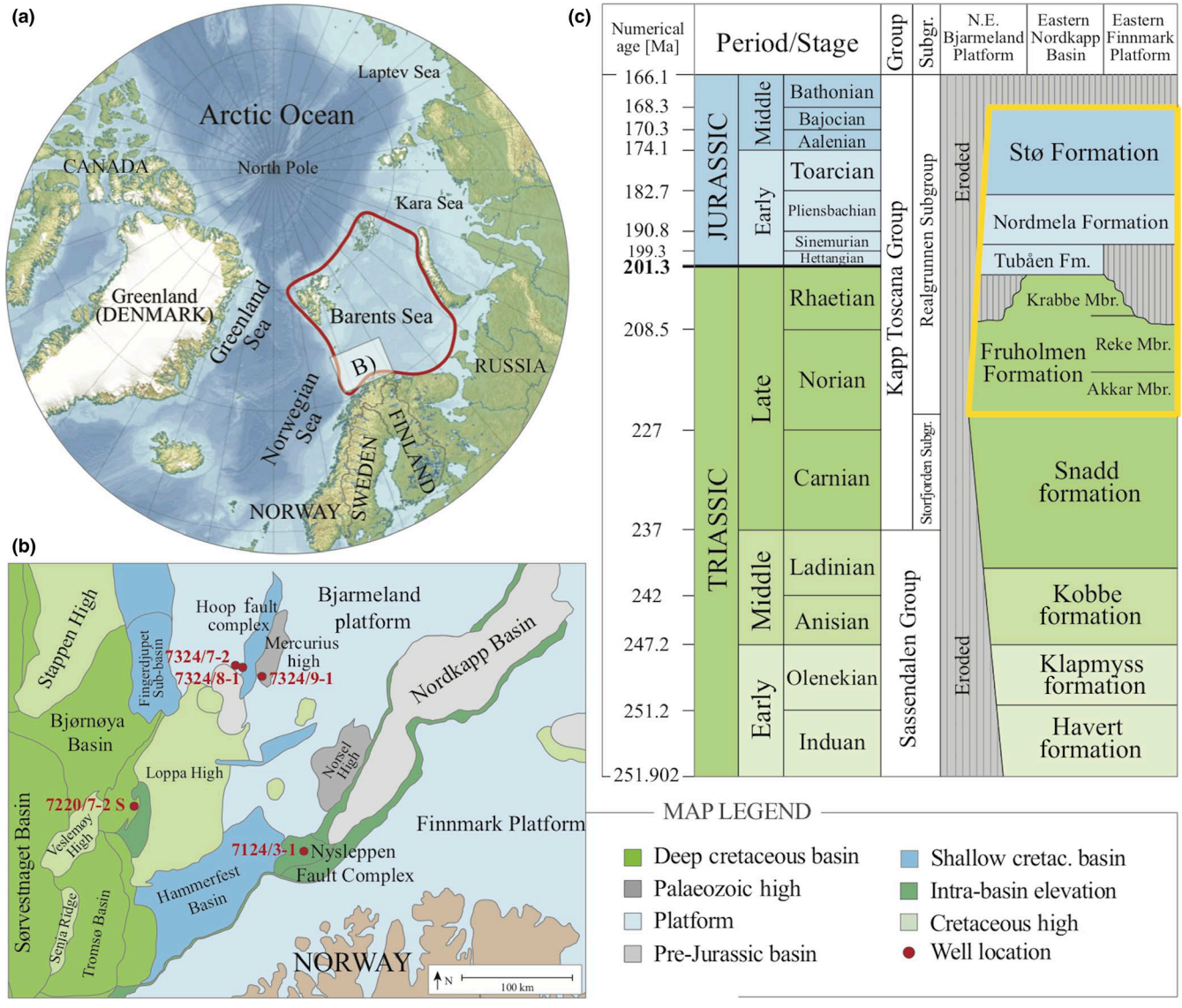

FIGURE 1 The greater Barents Sea is situated along two shear margins separating the Norwegian Sea and Greenland Sea from the Arctic Ocean in the north (a). The well database is located in the southwestern Barents Sea basin, which is characterized by a fan-shaped array of NE–SW oriented half-grabens and structural highs (b). Formations of the Realgrunnen Subgroup comprise the lithostratigraphic interval of interest in this study (c). Figures are modified from Vigran (2014), Cohen, Harper, and Gibbard (2018), Arctic Ocean relief location map.png. (2014) and NPD Factmaps (2019)

sediments (Worsley, 2008). The Barents shelf has also been affected by at least three episodes of regional-scale magmatism: the Siberian Traps Large Igneous Province (LIP) at the Permian–Triassic transition, the High Arctic LIP during Early Cretaceous and the North Atlantic rifting at the Paleocene–Eocene transition (Faleide et al., 2018).

The Triassic–Jurassic succession in the SWBSB was deposited on an epicontinental platform located between 45° and 70°N (Scotese, 2004). During the Mesozoic, the Barents Sea platform was surrounded by hinterland massifs of the Greenland and Norwegian Caledonides to the west and southwest, Paleoproterozoic and Archean complexes of Fennoscandia to the south and the Uralide-Taimyr Orogen to the east. High subsidence rates following the mid-Permian rifting enabled deposition of thick, mudstone-dominated successions during Triassic. The distribution of compositionally mature sandstones was mainly restricted to the southern basin margins, where prograding, westward-dipping clinoforms constituting the Havert, Klappmyss and Kobbe formations thicken eastwards (Eide, Klausen, Katkov, Suslova, & Helland-Hansen, 2017; Worsley, 2008).

Moderately humid climate conditions in the Early-Middle Triassic were replaced by warmer and drier conditions in the Boreal region during most of the Middle-Late Triassic (Hochuli & Vigran, 2010; Mangerud & Rømuld, 1991). During deposition of the Snadd Formation, the SWBSB was dominated by extensive delta progradation from the southeastern Uralide Orogeny. Overall coarsening-upwards sequences range from offshore shales, through shallow marine to fluvial sandstones with predominantly immature compositions (Klausen, Ryseth, Helland-Hansen, Gawthorpe, & Laursen, 2015; Mørk, 1999). High concentrations of unstable lithic components have often been attributed to the bedrock lithology of the southeastern hinterland (Fleming et al., 2016; Line, Jahren, & Hellevang, 2018), although the mineralogy of the Polar Uralides is scarcely documented in published literature. In Late Carnian–Early Norian, significant changes in fluvial channel body geometries are interpreted to reflect changes in the hinterland to the southeast (Klausen, Ryseth, Helland-Hansen, Gawthorpe, & Laursen, 2014). Palynological and sedimentological evidence also record a humidity increase in the Boreal realm in the Late Triassic (Hochuli & Vigran, 2010; Ryseth, 2014).

An Early Norian flooding surface caps the Snadd Formation and marks the base of the final, widespread progradational unit of the Triassic high-accommodation basin: the Norian–Rhaetian Fruholmen Formation. At the southern basin margin, a strong petrographic contrast is documented between litharenithic sandstones of the Snadd Formation and mature quartz arenites of the Fruholmen Formation (Fleming et al., 2016). This contrast has been referred to as the most significant petrographic turn-over in the Arctic region (Bergan & Knarud, 1993; Mørk, 1999). Similar to the Snadd Formation below, the Fruholmen Formation comprises a lower, coarsening upwards interval of dark mudrocks and sandstones, overlain by coal-bearing, heterolithic deposits (Ryseth, 2014). Although the Fruholmen Formation exceeds 200 m in the Hammerfest Basin, the succession is poorly defined in seismic from platform areas and highs due to numerous erosional hiatuses and significant thickness variation (Müller et al., 2019).

Most of the accommodation space left by Late Paleozoic structural lows and Permian carbonate reef platforms was filled during the Triassic. In the earliest Jurassic, high accommodation and sedimentation rates were replaced by limited accommodation and bypass. Decreasing subsidence rates in the SWBSB were accompanied by paleogeographic re-configurations and rejuvenation of hinterlands to the south (Ryseth, 2014). As syn- and post-depositional uplift and erosion have left the Upper Triassic and Jurassic successions partially preserved and condensed on platform areas and structural highs, regional investigations have proven difficult using conventional seismic (Klausen, Müller, Slama, & Helland-Hansen, 2017). However, a recent study equipped with high-resolution P-Cable seismic documented regional angular unconformities between the Upper Triassic and Lower Jurassic strata across the Barents shelf that were linked to the development of forebulge uplift related to the Novaya Zemlya fold-and-thrust belt in the eastern part of the Barents Sea (Müller et al., 2019). This far-field compressional stress is postulated to have facilitated the transition from high- to low-accommodation settings in the SWBSB, and thereby reworking of uplifted Triassic strata and mixing of sediment with Uralide, Caledonian and Fennoscandian provenance signatures.

3 | MATERIALS AND METHODS

The present study is based on observations and samples from core material from five wells in the SWBSB (Figure 1b). 560 m of core from the Fruholmen, Tubåen, Nordmela and Stø formations were logged, where lithology, grain size, sedimentary structures, unit thicknesses and unit boundaries constituted the basis for sedimentological interpretations. Formation boundaries were defined based on available biostratigraphic reports. Collected petrography samples were prepared and analysed at the Department of Geoscience, University of Oslo. Preparation and analysis of detrital zircon grains were conducted at the Department of Earth Science, University of Bergen.

In all, 84 core samples were prepared for Powder X-ray diffraction (XRD). Raw data diffractograms, preparation and instrumental details are listed in supplementary material. Rietveld refinement in BGMN-Profex was used to model the relative amounts of mineral phases from bulk XRD data. Modelling results were normalized after excluding mineral remnants from the drilling fluid and core flushing.

In all, 74 epoxy-impregnated thin sections were prepared for optical microscopy. Oil-stained sandstone samples were washed prior to epoxy impregnation by solvent separation of dichloromethane (DCM + MeOH) with a volume ratio of 93:7 and left to soak for approximately 24 hr. Compositional and textural analyses were conducted through point count analyses of 300 counts per thin section. Framework grains were classified as monogranular quartz, feldspars (plagioclase and K-feldspar) and polygranular rock fragments after Dott (1964). For compositional classification, mica grains and completely dissolved or recrystallized framework grains (pseudomorphous replacements, as described in Wilson & Pittman, 1977) were treated as part of the rock fragment assembly. The amount and distribution of argillaceous matrix were quantified through modal analysis. Grain sizes were registered by measuring the longest axis of >100 grains per sample, and the roundness and sphericity of framework grains were classified in accordance with the roundness scale after Powers (1953). Counts were normalized to 100% and averaged for each formation.

Mineral compositions of argillaceous material were identified using scanning electron microscopy (SEM). SEM analyses were performed on a subset of 17 carbon-coated thin sections using a Hitachi SU5000 FE-SEM (Schottky FEG) scanning electron microscope with a Bruker XFlash30 EDS.

A subset of nine samples were prepared for detrital zircon age analysis. To link petrographic characteristics to geochronological provenance data, samples collected for detrital zircon age analysis were taken from the same depth intervals as the petrographic samples. The samples were hand-crushed, and individual zircon grains were mounted in 1-inch epoxy-filled blocks and polished to expose surfaces for cathodoluminescence imaging and laser-ablation. A Nu AttoM high-resolution ICP-MS coupled to a 193 nm ArF excimer laser (Resonetics RESOlutionM-50 LR) was used to measure the Pb/U and Pb isotopic ratios in zircons. No common Pb correction was applied to the data. The concordance-discordance criterion used herein is 10%. Histograms and probability density plots (PDP) were generated with the ISOPLOT program v. 3.70 (Ludwig, 2008).

4 | RESULTS

4.1 | Sedimentary facies associations

A diverse sedimentary facies assembly ranging from marine to continental environments is documented in the cored sections (Figure 2) and summarized in Table 1. Core photo references are provided in supplementary material.

Fining upwards sandstone units with root structures and coal intervals documented in the Snadd Formation from the southern basin margin are interpreted to record continental floodplain facies (Figure 2a). These are overlain by bioturbated, coarsening upward sandstone units interpreted as marginal-marine facies, observed below the Early Norian flooding surface. The Norian–Rhaetian Fruholmen Formation displays a regressive facies trend, with shaly prodelta and sandy, upwards-coarsening and bioturbated delta front deposits at the base. These deposits are overlain by stacked braided and distributary channels and floodplain facies, as indicated by interdistributary bay, small channel- and overbank deposits. The Tubåen Formation comprises stacked successions of cross-stratified and coarse-grained braided channel deposits, as indicated by coarse and imbricated pebbles.

In the west, the Fruholmen Formation shows a more heterolithic signature with bioturbation, some root structures and syneresis cracks indicative of tidal influence (Figure 2b). The topmost 15 m below the Triassic–Jurassic boundary consist of cross-stratified, fine sandstone with mud stringers and pyrite concretions (outlined in yellow frame, Figure 2b), suggesting a channelized feature with tidal influence. Above the Triassic–Jurassic boundary, the Hettangian Tubåen Formation displays medium-grained and cross-stratified sandstone units indicative of braided channels. Mixed tidal flat facies were recognized by heterolithic lithologies, syneresis cracks, coal bed and root structures.

Core from the Fruholmen Formation in the northern basin interior consists primarily of continental and marginal-marine facies, including meandering channel systems and point bars with rip-up mud clasts, ripple-laminated levee deposit and heterolithic mixed tidal flat facies (Figure 2c). In the Hoop Fault Complex, the transition into the Pliensbachian Nordmela Formation is characterized by a thin, erosive and very coarse-grained lag deposit, overlain by an extensively bioturbated and upwards-coarsening shoreface deposit. At the base of the Toarcian Stø Formation, a 5-m thick, medium-grained sandstone interval is subdivided into multiple fining-upwards units containing pebble-sized clasts at the base, overlain by cross-stratified and bioturbated sandstone. Similar facies characteristics are documented from Early Jurassic strata on East-Greenland, where the individual fining-upwards units are interpreted as transgressive lags covered by wave/tide-influenced cross-beds (Eide et al., 2016). In the Hoop Fault Complex, the transgressive deposits are overlain by a fine-grained and cross-bedded section with weak bioturbation, interpreted as a channel fill deposit.

At the Mercurius High, a cross-stratified, fine-grained sandstone unit of the Norian Fruholmen Formation is interpreted to represent parts of a meandering channel system (Figure 2d). A vertical burrow structure at the top of a fining-upwards channel deposit indicate tidal influence (outlined in yellow, Figure 2d). Above the Triassic–Jurassic boundary, the Pliensbachian Nordmela Formation displays a fining-upwards trend. Based on the clay stringers and basal mud chips, the Nordmela Formation was interpreted as a tidal channel in this core. The clay-rich and intensely bioturbated lowermost Stø Formation was interpreted as offshore transition facies,

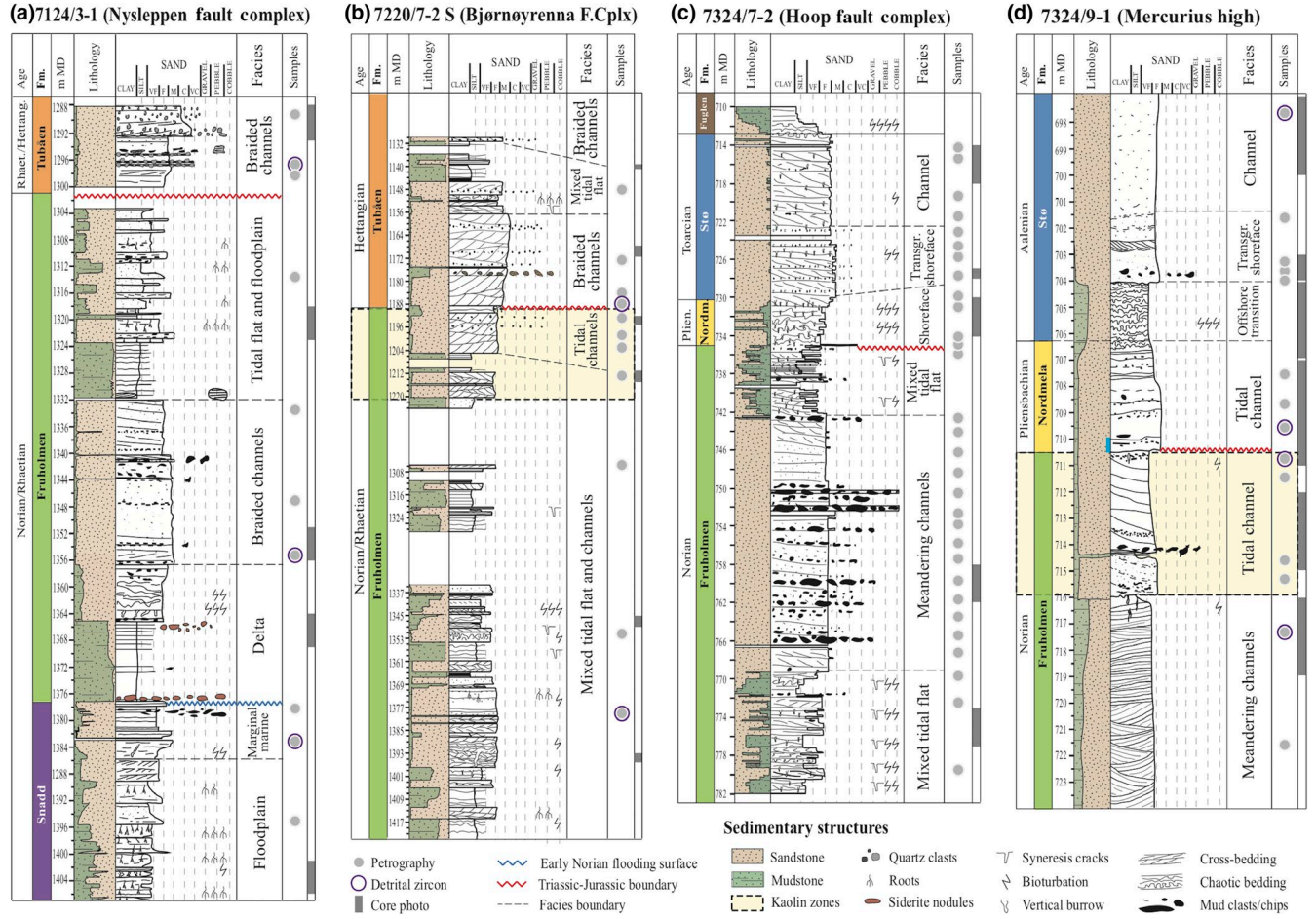

FIGURE 2 Summary of interpreted sedimentary facies and sampled intervals from the Snadd, Fruholmen, Tubåen, Nordmela and Stø formations in the Nysleppen Fault Complex (a), Bjørnøyrenna Fault Complex (b), Hoop Fault Complex (c) and Mercurius High (d). As the cored sections in wells 7324/8-1 and 7324/7-2 from the Hoop Fault Complex display similar facies distributions, only 7324/7-2 is presented in the figure. Kaolin-enriched intervals below the Triassic–Jurassic boundary are indicated in yellow. Referenced core photos are found in supplementary material

which is erosively overlain by another lag deposit similar to the one described from the Hoop Fault Complex, which contains coal fragments and intra-formational clasts. As the topmost fine-grained and massive sandstone in this core contains coal fragments and lacks marine trace fossils, this section of the Stø Formation is interpreted to represent a fluvial channel fill.

4.2 | Petrographic signatures across the Triassic–Jurassic boundary

4.2.1 | Southern basin margin

A sharp contrast was documented between the mineralogically diverse Snadd Formation and the extremely quartz-rich Fruholmen Formation in the southern basin location (outlined by dashed yellow lines in Figures 3a–c and 4c). Rock fragments are scarce (1%–3%) above and below the Early Norian flooding surface and the assemblies consist solely of mica. Although grain sizes vary from fine sand to coarse silt in both Triassic formations (Figure 3b), minerals that characterize the Snadd Formation sandstones (chlorite, siderite, pyroxene and fluorapatite) are absent above the Early Norian transgressive surface (Figure 3c). The braided channel deposits in the Fruholmen Formation contain only quartz, plagioclase and traces of kaolin (Figure 4c), whereas the stacked distributary channels above contain additional muscovite/illite, K-feldspar and significantly higher kaolin content (20%–40%; Figure 4b).

Apart from minor grain size differences, no significant contrast is registered between the Fruholmen and Tubåen formations in the south (Figure 4a–c). Extreme compositional maturity is registered on either side of the Triassic–Jurassic boundary (overlapping compositions in Figure 3a) and the formations are only distinguished by a larger grain size diversity and higher kaolin content in the Fruholmen Formation. The braided channel facies in the Fruholmen Formation contains slightly higher plagioclase content compared to the braided channels in the Tubåen Formation.

TABLE 1 Facies characteristics in the Realgrunnen Subgroup from the cored sections

Environment	Facies	Interpretation	Grain size and structures	Occurrence
Marine	1	Offshore transition	Clst[1], extensive bioturb[14].	Stø
	2	Delta	Vfs[2], CU[7], bioturb, coal, sid[10]	Fruholmen
	3	Shoreface	Vfs, extensive bioturb.	Snadd, Nordmela
Marginal marine	4	Mixed tidal flat	Vfs, heterolithic, syn[9], bioturb.	Fruholmen
Foodplain	5	Floodplain shale	Clst, PPL[13]	Fruholmen
	6	Crevasse splay	Vfs, coal, current ripples, roots	Snadd, Fruholmen
Channels	7	Tidal channel	Vfs-fs[3], FU[8], coal, bioturb., calc[11]	Fruholmen, Nordmela
	8	Meandering channels	Fs-ms[4], rip-up clasts, coal, cross-bedding.	Snadd, Fruholmen, Stø
	9	Braided channels	Ms-cs[5], qz[12] clasts, coal.	Fruholmen, Tubåen, Stø
Transgressive lag	10	Lag deposits	Ms-vcs[6], pebble clasts, cross-bedding.	Nordmela, Stø

[1]Claystone, [2]Very-fine sand, [3]Fine sand, [4]Medium sand, [5]Coarse sand, [6]Very coarse sand, [7]Coarsening upward, [8]Fining upward, [9]Syneresis cracks, [10]Siderite, [11]Calcite, [12]Quartz, [13]Plane-parallel lamination, [14]Bioturbation.

4.2.2 | Western basin interior

Rhaetian Fruholmen Formation sandstones in the western basin interior are characterized as subarkoses to sublitharenites, with grain sizes varying from very fine sand to coarse silt (outlined by dashed blue lines in Figures 3d–f and 4e–f). The rock fragment assembly contains scarce distributions (<2%) of mica and mudrock fragments. One sample contains 15% chert. The mineral assembly includes quartz, plagioclase, K-feldspar, muscovite/illite and kaolin, where plagioclase appears to be slightly favoured over K-feldspar (Figure 3f). Biotite, calcite, siderite and pyrite were registered in trace amounts. A distinct increase in the kaolin content is documented just below the Triassic–Jurassic boundary (indicated by arrow in Figure 3f). This interval is annotated by a yellow frame in Figure 2b.

The mineralogical and textural contrasts between the subarkosic–sublitharenitic Fruholmen and the quarzitic Tubåen formations in the west are dramatic (Figure 3d–f). Rock fragments are generally absent in the Tubåen Formation but traces (<1%) of chert, mica and pseudomorphous replacements have been observed. The bulk mineral assembly in the Tubåen Formation consists exclusively of quartz and traces of plagioclase, K-feldspar and kaolin (Figure 3f). Quartz arenites display two distinct grain size populations: medium sand and very fine sand (Figure 4d).

4.2.3 | Northern basin interior

Two distinct sandstone signatures were detected in the Fruholmen Formation in the northern basin interior. The most abundant northern assembly (annotated N) classifies as a subarkose to lithic subarkose and occurs at the Hoop Fault Complex and Mercurius High (outlined by dashed red lines in Figures 5 and 6c–d). The rock fragment assembly averages at 10% and contains primarily mica and mudrock fragments. Iron-bearing minerals and significant amounts of argillaceous pore-fill characterize the samples from this assembly (Figure 6h). Individual samples are moderately to well sorted and grain sizes range from coarse silt to fine sand (Figure 5b; red polygon in Figure 5e). A diverse mineral suite is registered from the bulk XRD analyses (Figure 5c,f), with quartz abundances ranging from 45% to 70%. Feldspars account for 15%–25% of the bulk, with plagioclase-dominance over K-feldspar. Argillaceous minerals generally account for about 10%–30% of the bulk samples, where muscovite/illite and kaolin minerals dominate the clay mineral assembly (Figure 6c). Chlorite is the least abundant clay phase and accounts for about 2%–5% of the bulk. When present, chlorite is mostly distributed as pore-fill mixed with other clay-fraction particles (Figure 6h). Samples collected from cemented nodules contain 15%–20% calcite, and one sample contains 26% pyrite. Siderite is rarely found in samples containing calcite, and typically constitutes 2%–10%. Minor (<2%) quartz cement was detected in the northern petrographic assembly in the Hoop area (Figure 6d).

The second sandstone assembly in the Fruholmen Formation from the northern basin interior (annotated N2 and outlined by dashed bright red lines in Figure 5d–f) has a strong resemblance to the Norian–Rhaetian mineral assembly in the west and consists of well sorted fine to very-fine sand. This mineral suite occurs in the tidal channel facies at the Mercurius High, above sandstones of the iron-containing northern assembly and below the Triassic–Jurassic boundary (Figure 2d). In addition to micas and mudrock fragments, chert and pseudomorphous replacements are rock fragment constituents that distinguish the N2 suite from the ferric northern assembly. In contrast to the diverse mineral suite documented in the northern assembly below, ferric minerals are almost absent in the N2 assembly (Figure 5f). Quartz is

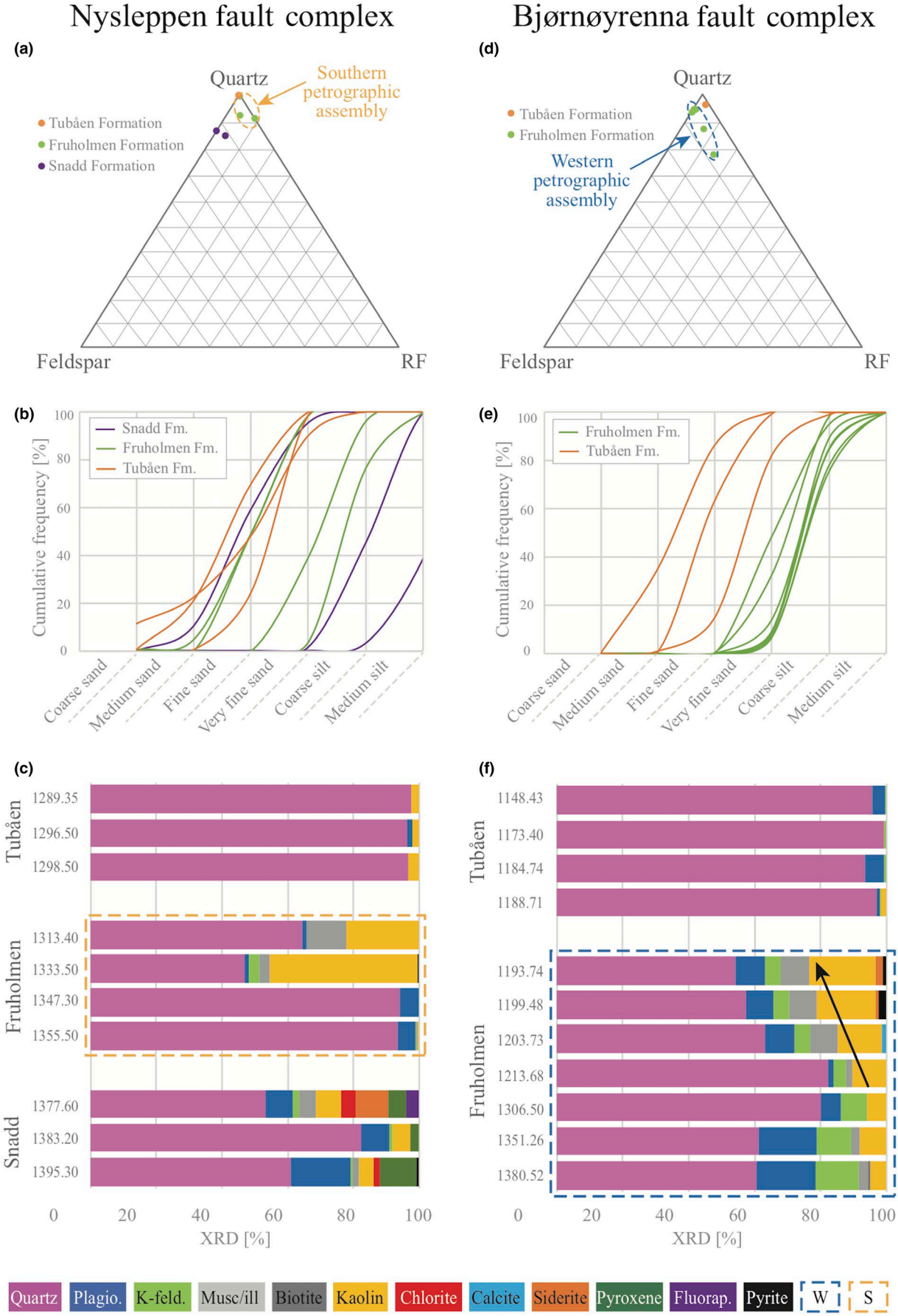
Nysleppen fault complex
Bjørnøyrenna fault complex
(a)
Quartz
Southern petrographic assembly
Tubåen Formation
Fruholmen Formation
Snadd Formation
Feldspar
RF
(d)
Quartz
Tubåen Formation
Fruholmen Formation
Western petrographic assembly
Feldspar
RF
(b)
Snadd Fm.
Fruholmen Fm.
Tubåen Fm.
Cumulative frequency [%]
Coarse sand
Medium sand
Fine sand
Very fine sand
Coarse silt
Medium silt
(e)
Fruholmen Fm.
Tubåen Fm.
Cumulative frequency [%]
Coarse sand
Medium sand
Fine sand
Very fine sand
Coarse silt
Medium silt
(c)
Tubåen
1289.35
1296.50
1298.50
Fruholmen
1313.40
1333.50
1347.30
1355.50
Snadd
1377.60
1383.20
1395.30
XRD [%]
(f)
Tubåen
1148.43
1173.40
1184.74
1188.71
Fruholmen
1193.74
1199.48
1203.73
1213.68
1306.50
1351.26
1380.52
XRD [%]
Quartz
Plagio.
K-feld.
Musc/ill
Biotite
Kaolin
Chlorite
Calcite
Siderite
Pyroxene
Fluorap.
Pyrite
W
S

FIGURE 3 Sampled sandstones of the Snadd, Fruholmen and Tubåen formations in the cores from the Nysleppen (a–c) and Bjørnøyrenna (d–f) fault complexes show distinct characteristics in composition, grain size and mineralogy. Elevated kaolin contents are registered in the upper Fruholmen Formation, towards the T–J boundary, in both locations. Sampled intervals are indicated in Figure 2a,b

the dominating mineral and the K-feldspar preference over plagioclase is another property that distinguishes the N2 sandstone suite from the northern assembly below and in the Hoop Fault Complex. The kaolin content increases up to 20% towards the Triassic–Jurassic boundary (Figure 6g; indicated with arrow in Figure 5f), while the total feldspar and muscovite/illite concentrations remain constant throughout the interval. This interval corresponds to the section framed in yellow in Figure 2d.

A sharp mineralogical contrast separates the Fruholmen and Nordmela formations in the northern basin interior (Figure 5c,f). Sandstones representing the Nordmela Formation are classified as sublitharenites in the Hoop Fault Complex (Figure 5a), and occasionally as quartz arenites at the Mercurius High (Figure 5d). A relatively wide range of rock fragments were detected from the Nordmela Formation; chert, mica, mudrock fragments, pseudomorphous replacements and rutile were observed in minor amounts (<3%). The fine to very fine grain sizes are coarser compared to the northern petrographic assembly in the Fruholmen Formation (Figure 5b) but share similar grain size distributions with the N2 petrographic assembly (bright red polygon in Figure 5e). The mineral suite of the Nordmela Formation sandstones in the Hoop area includes quartz, K-feldspar, muscovite/illite and kaolin, with traces of plagioclase, chlorite, calcite and rutile (Figures 5c and 6b). At the Mercurius High, the Nordmela Formation contains quartz and plagioclase, with minor amounts of K-feldspar and grain-coating kaolin (Figures 5f and 6f).

Another mineralogical maturity increase is associated with the Nordmela-Stø transition, where most Stø Formation sandstones plot as quartz arenites (Figure 5a,d). Few rock fragments are encountered in the Stø Formation (3% on average), and traces of chert, mica, mudrock fragments, pseudomorphous replacements and pyritic clasts (Figure 6e) occur sporadically in individual samples. Increased mineralogical maturity and sorting is coupled with an overall grain size increase in Hoop (Figure 5b), while overlapping grain size distributions are documented at the Mercurius High (Figure 5e). In addition to the quartz-dominance (>90%), sandstones from

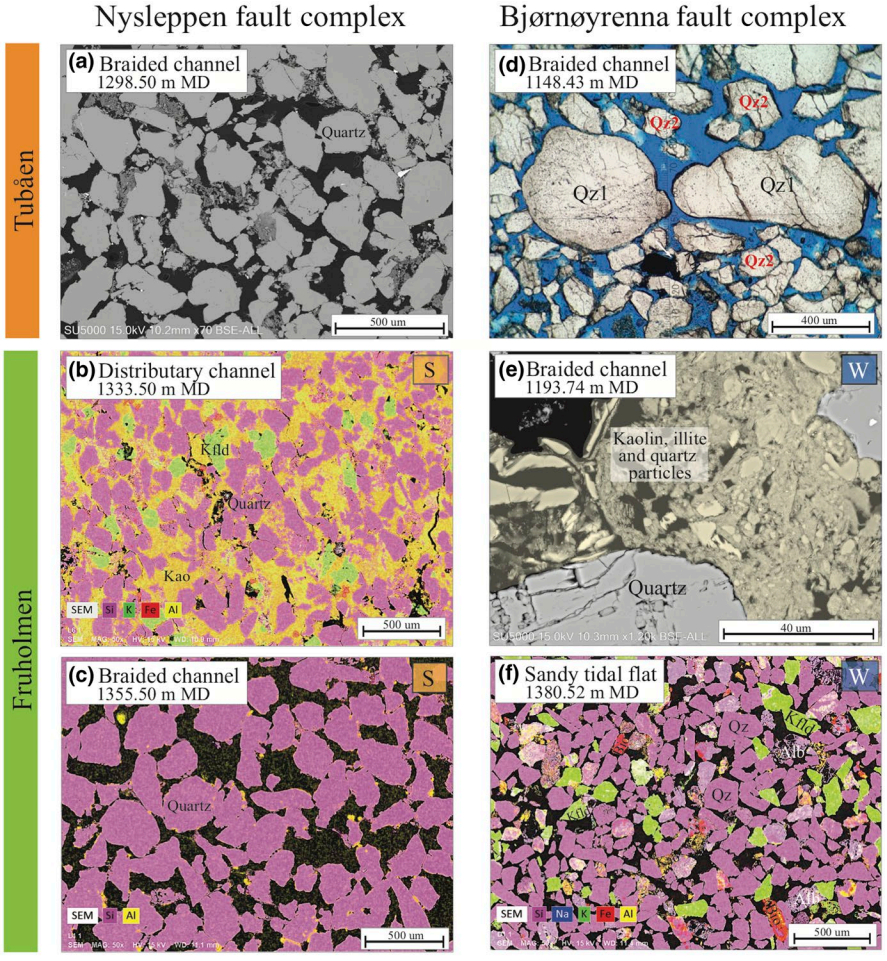

FIGURE 4 Characteristics of the Fruholmen and Tubåen formations in the Nysleppen (a–c) and Bjørnøyrenna (d–f) fault complexes are visualized by SEM micrographs, elemental distribution maps and thin section images. Samples from the top Fruholmen Formation show a dominance of Al-rich pore-fill (indicated in yellow) (b). The pore-fill consists of clay-fractioned quartz mixed with poorly developed crystals of illite and kaolin (e). Extreme compositional maturity characterizes the southern assembly of the Fruholmen Formation (indicated S) (c), whereas a more feldspatic composition is registered in the western assembly (indicated W) (f). The Tubåen Formation in the western basin interior displays two distinct and rounded grain size populations (Qz1 and Qz2) (d), whereas a homogeneous assembly of angular grains is recorded in the south (a). Alb, Albite; Bio, Biotite; Kao, kaolin; Kfld, K-feldspar; Qz, quartz

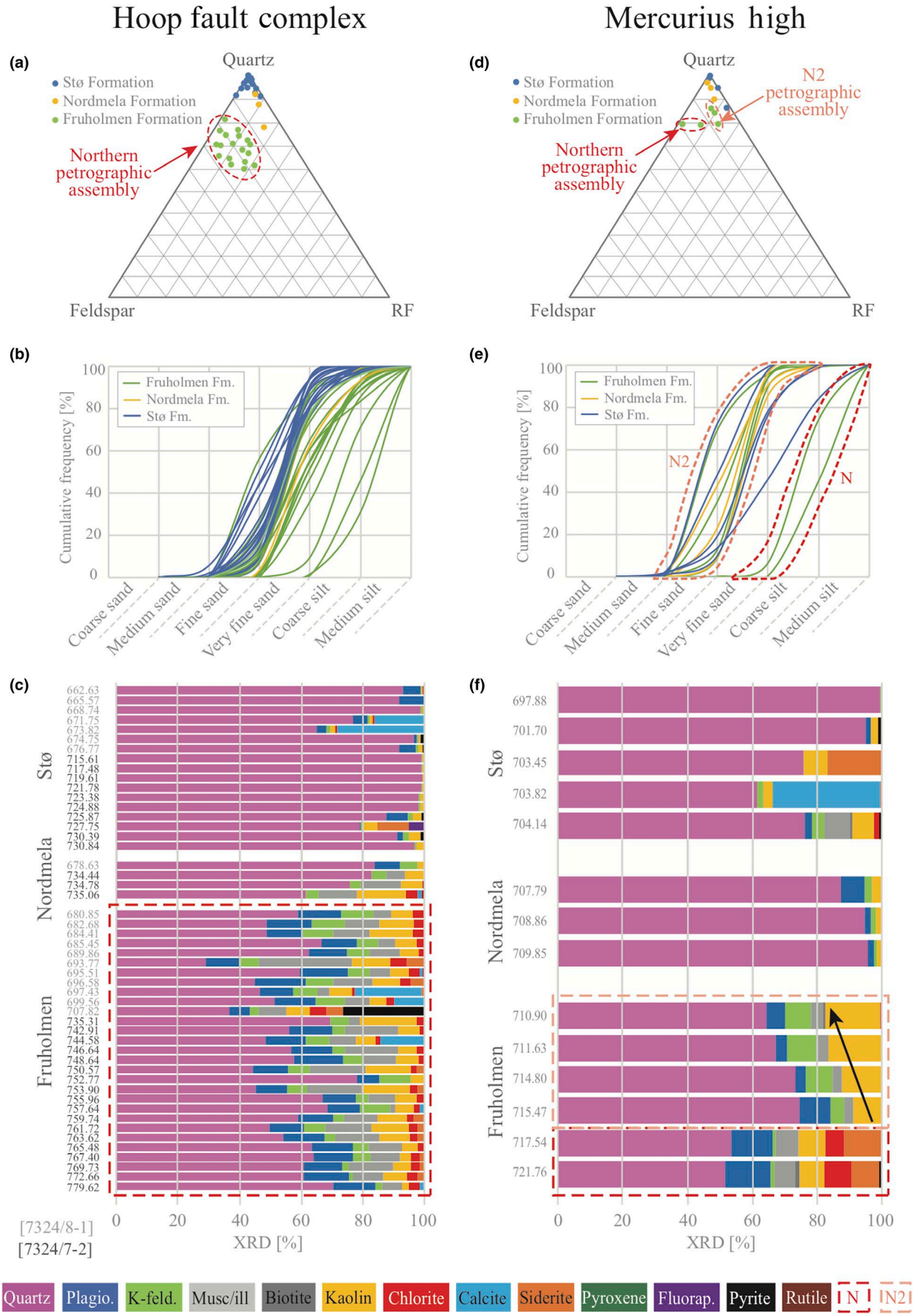
Hoop fault complex
Mercurius high
(a)
Quartz
Stø Formation
Nordmela Formation
Fruholmen Formation
Northern petrographic assembly
Feldspar
RF
(d)
Quartz
Stø Formation
Nordmela Formation
Fruholmen Formation
N2 petrographic assembly
Northern petrographic assembly
Feldspar
RF
(b)
Cumulative frequency [%]
Fruholmen Fm.
Nordmela Fm.
Stø Fm.
Coarse sand
Medium sand
Fine sand
Very fine sand
Coarse silt
Medium silt
(e)
Cumulative frequency [%]
Fruholmen Fm.
Nordmela Fm.
Stø Fm.
N2
N
Coarse sand
Medium sand
Fine sand
Very fine sand
Coarse silt
Medium silt
(c)
Stø
Nordmela
Fruholmen
662.63
665.57
668.74
671.75
673.82
674.75
676.77
715.61
717.48
719.61
721.78
723.38
724.88
725.87
727.75
730.39
730.84
678.63
734.44
734.78
735.06
680.85
682.68
684.41
685.45
689.86
693.77
695.51
696.58
697.43
699.56
707.82
735.31
742.91
744.58
746.64
748.64
750.57
752.77
753.90
755.96
757.64
759.74
761.72
763.62
765.48
767.40
769.73
772.66
779.62
[7324/8-1]
[7324/7-2]
XRD [%]
(f)
Stø
Nordmela
Fruholmen
697.88
701.70
703.45
703.82
704.14
707.79
708.86
709.85
710.90
711.63
714.80
715.47
717.54
721.76
XRD [%]
Quartz
Plagio.
K-feld.
Musc/ill
Biotite
Kaolin
Chlorite
Calcite
Siderite
Pyroxene
Fluorap.
Pyrite
Rutile
N
N2

FIGURE 5 The composition, grain size and mineralogy of the Fruholmen, Nordmela and Stø formations in the Hoop Fault Complex (a–c) and Mercurius High (d–f) in the northern basin interior reveal two distinct mineralogical suites in the Fruholmen Formation; the northern assembly (indicated by dashed red lines) and the N2 assembly (indicated by dashed light red lines), which only occurs at the Mercurius High. Increasing kaolin contents are registered towards the T–J boundary in samples from the 7324/9-1 core. Sampled intervals are indicated in Figure 2c,d

the basal lag deposit contain minor amounts of feldspars, muscovite/illite, kaolin, calcite and siderite (Figures 5c,f and 6a). Trace amounts of chlorite, fluorapatite, pyrite and rutile were also detected from XRD. Calcite and siderite occur as pore-filling cements, while pyrite crystals were found in concentric laminae around detrital quartz grains in the transgressive lag deposit at the Mercurius High (Figure 6e).

4.3 | Detrital zircon age signatures

Results from the detrital zircon age analyses are listed in the supplementary material and summarized in Figure 7. Grains with age signatures from 270 to 350 Ma are attributed to the Uralian Orogeny, whereas the Fennoscandian provenance includes catchment areas with Meso- and Neoproterozoic sedimentary rocks from northern Finnmark and Archean to Paleoproterozoic rocks of the Fennoscandian Shield (Klausen et al., 2017). This provenance signature shows a distinct lack of zircon ages younger than the Cambrian. A third provenance, referred to as Caledonian, is characterized by Paleozoic peaks mixed with Mesoproterozoic ages.

4.3.1 | Southern basin margin

Floodplain deposits within the Snadd Formation at the southern basin margin comprise detrital zircon grains ranging from Late Triassic to Archean(?) in age. Histograms and frequency spectrums reveal an abundance of grains younger than Permian (Figure 7c). This signature is significantly younger than the Caledonian and commonly associated with provenance areas in the southeast and east Uralides (Fleming et al., 2016). However, we note a peak of grain ages older than 500 Ma which likely has a source in the Timanide orogen and is interpreted to represent sediments from the southern- and southeastern margins of the basin.

In strong contrast to the Uralide age signatures documented in the Snadd Formation, detrital zircon grains from the overlying Fruholmen Formation show typical Fennoscandian age signatures, lacking grains younger than 500 Ma (Figure 7b). No grains approximate the maximum depositional age.

The braided channel of the Tubåen Formation contains detrital zircon age signatures attributed to the Sveconorwegian and Svecofennian orogenies exclusively, with a minimum age peak at 900 Ma (Figure 7a). Accordingly, we associate these age peaks with the Fennoscandian hinterland.

4.3.2 | Western basin interior

In the Fruholmen Formation in the west, the youngest recorded age (196.2 ± 5.7 Ma) is close to the maximum depositional age of the formation and a significant contribution of Caledonian ages are also registered (Figure 7e).

Fluvial deposits of the Tubåen Formation show Fennoscandian and Caledonian age signatures characterized by grains with ages from 1,000 to 1,600 Ma (Figure 7d). This signature is attributed to the Sveconorwegian orogen and its associated metasediments. Age signatures from 1,750 to 2,000 Ma are typical for the Svecofennian orogen, and a Caledonian age peak and grains as young as Late Carboniferous are also recorded.

4.3.3 | Northern basin interior

Young detrital age signatures (<350 Ma) documented in all samples from the basin interior are considered as typical for Uralian provenance areas (Bue & Andresen, 2014). However, extensive recycling has been documented within the Fruholmen Formation and these zircon grains may thus have been recycled from younger Triassic formations (Fleming et al., 2016). In addition to pronounced Uralian age peaks, the Fruholmen Formation from the Hoop Fault Complex shows minor contribution of Caledonian age signatures (Figure 7h). The youngest grain encountered in this sample (213.8 ± 5 Ma) approximates the depositional age of the formation; however, the possibility of lead loss cannot be discounted. Through cathodoluminescence imaging, prismatic and oscillatory-zoned zircon grains younger than 230 Ma display sector-zoned inner domains and inherited cores (Figure 7h'), suggesting an igneous origin (Klausen et al., 2017).

By contrast, Caledonian age peaks are absent in the lowermost Fruholmen Formation channel at the Mercurius High (Figure 7l). It should, however, be noted that the number of validated analyses in this sample ($n = 33/64$) is considered statistically insignificant. The sample from the N2 assembly, on the other hand, reveals dominant age peaks associated with the Uralian, Caldeonian and Svecofennian orogenies (Figure 7k). Norian zircon grains were also recorded from this interval.

The detrital zircon age spectra from the Pliensbachian Nordmela Formation in the basin interior is characterized by Triassic zircon grains and notable Caledonian age peaks (Figure 7g,j). We also detected subtle Sveconorwegian and Svecofennian age peaks.

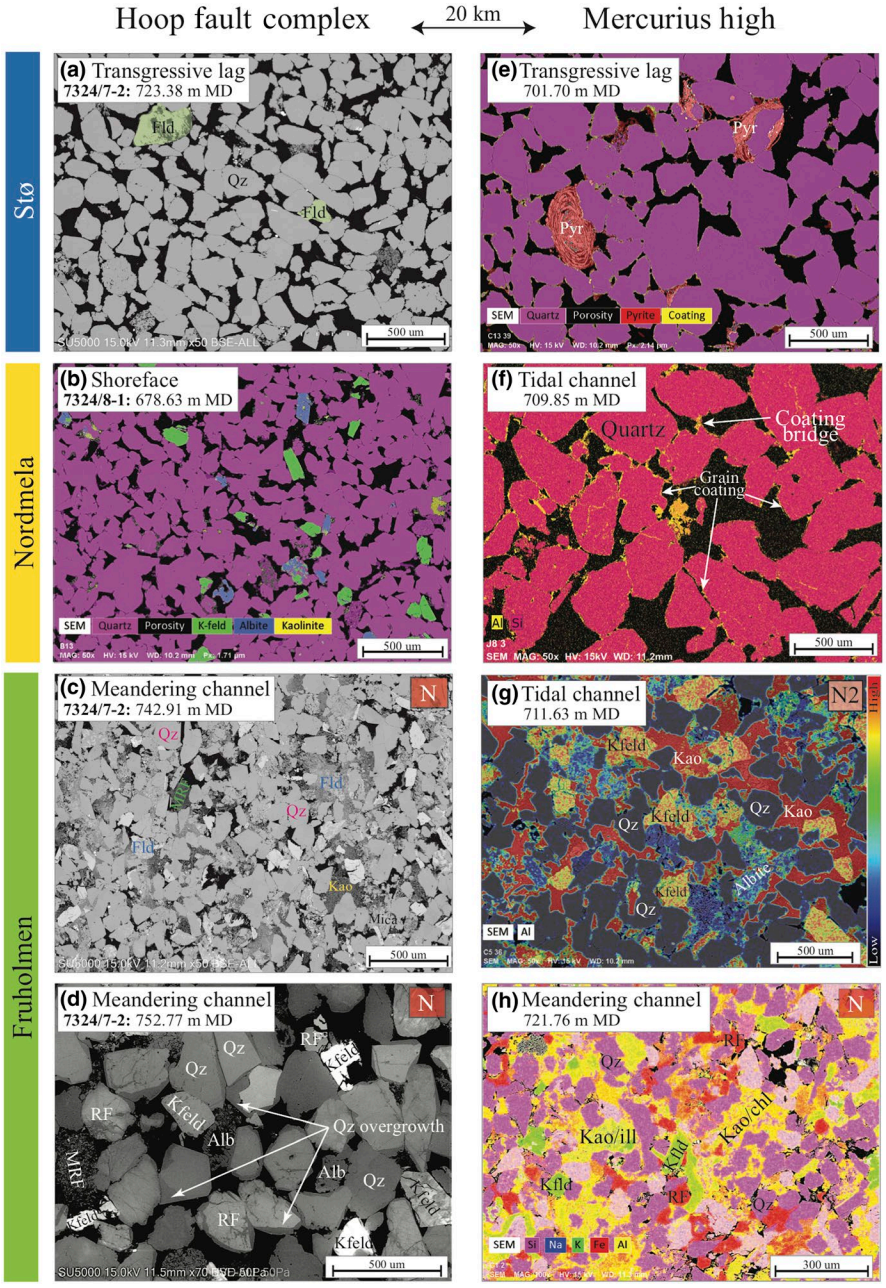

FIGURE 6 SEM micrographs and elemental maps visualize the contrasts between the mineralogically mature Stø and Nordmela formations, and the subarkoses of the Fruholmen Formation in the Hoop Fault Complex (a–d) and the Mercurius High (e–h). The northern assembly of the Fruholmen Formation (annotated N) occurs in both locations, whereas the compositionally more mature N2 assembly occurs only at the Mercurius High, where kaolinite dominates the pore space (g). Alb, Albite, Ill, illite, Kao, Kaolin, Kfld, K-feldspar, MRF, mudrock fragment, Pyr, pyrite, Qz, quartz, RF, rock fragment

The recorded isotope ages from the Stø Formation in the Hoop Fault Complex are characterized by abundant Triassic zircon grains in the Toarcian level (Figure 7f), which is distinctly different from the Caledonian and Fennoscandian signatures recorded in the Aalenian part of the Stø Formation from the neighbouring 7324/9-1 well on Mercurius High (Figure 7i).

5 | DISCUSSION

Detrital zircon and petrography characteristics reflect significant variations in sediment dispersal patterns to the SWBSB across the Triassic–Jurassic boundary. Compositional contrasts may therefore be discussed in terms of geographical and temporal variations in provenance, climate and basin configuration.

5.1 | Geographical and temporal provenance variations

Variations in sediment dispersal patterns from Middle Triassic to Early Jurassic are summarized and discussed with reference to conceptual paleogeographic reconstructions for the SWBSB (Figure 8). In the Middle-Late Triassic, during the deposition of the Kobbe and Snadd formations, the SWBSB was dominated by extensive delta progradation from

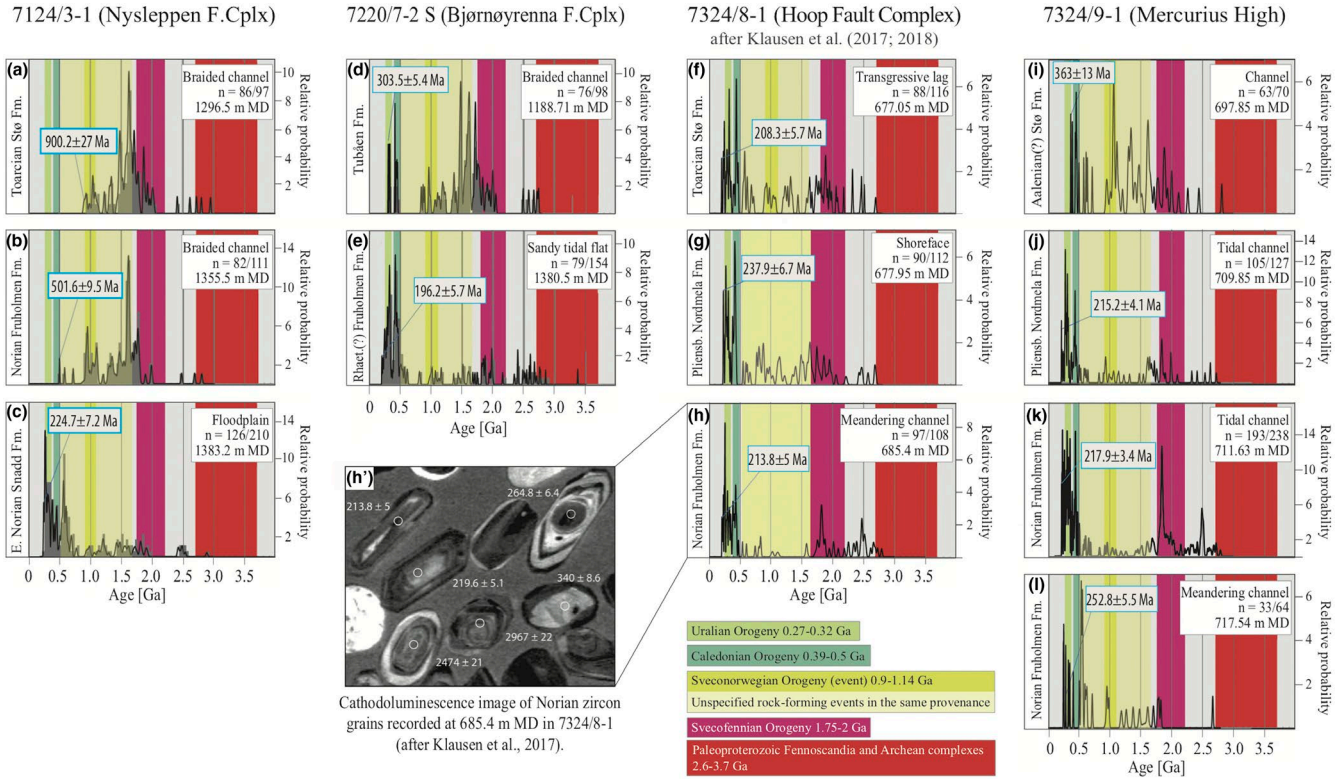

FIGURE 7 Probability density plots of detrital zircon ages recorded in the Snadd, Fruholmen, Tubåen, Nordmela and Stø formations from the Nysleppen (a–c), Bjørnøyrenna (d–e) and Hoop (f–h; Klausen et al., 2017, 2018) fault complexes, and at Mercurius High (i–l). Minimum ages are provided for each sample. The Fruholmen Formation display young zircon ages (196.2 ± 5.7 Ma) in the west (e), while the youngest zircon age detected in the southern location is 501.6 ± 9.5 Ma (b), indicating a different provenance for the Fruholmen Formation in the south. Cathodoluminescence imaging of Norian (210–230 Ma) zircon grains in the Hoop Fault Complex (h') suggests an igneous origin (Klausen et al., 2017). The Aalenian(?) Stø Formation in 7324/9-1 (i) shows Caledonian age signatures with a notable absence of young age signatures that are found in the underlying Nordmela (j) and Fruholmen (k) formations, and in the Toarcian Stø Formation in 7324/8-1 (f)

the southeastern Uralide Orogeny (Figure 8a; Glørstad-Clark, Faleide, Lundschien, & Nystuen, 2010). As a consequence of high rates of sedimentation and subsidence, the basin infill is characterized as compositionally immature. Sandstones were concentrated in deltaic and channelized deposits (indicated in dark red, Figure 8a) encased within fine-grained siliciclastics (Henriksen et al., 2011; Klausen et al., 2015). Sandstones deposited along the southern basin margin are described as compositionally mature, with good to excellent reservoir quality (Fleming et al., 2016). These properties have been linked to denudation of the Caledonides and the Precambrian basement rocks in Fennoscandia (Bergan & Knarud, 1993). Sediment supply from the southern hinterlands was likely limited and restricted to the southern margins of the basin (indicated in yellow, Figure 8a).

During deposition of the Norian–Rhaetian Fruholmen Formation, the basin configuration and sediment dispersal patterns that had dominated the SWBSB for 25 million years started to change (Figure 8b). Rejuvenation of the Caledonian and Fennoscandian hinterlands towards the end of the Triassic (Ryseth, 2014) introduced coarse-grained and quartz-rich sediments to the proximal basin margins in the south (indicated in yellow, Figure 8b), in strong contrast to the fine-grained lithic arkoses and litharenithic detritus that had dominated the basin since the Early Triassic. Bergan and Knarud (1993) were the first to characterize the petrographic shift across the Early Norian flooding surface as the most distinct and regionally important change in sandstone compositions in the Arctic. They attributed the compositional turn-around to extensive reworking of older Triassic strata and changing environments following the Early Norian transgression. Decreasing subsidence rates at the turn of the Norian were postulated to have facilitated repeated reworking and textural and mineralogical maturation of the Fruholmen Formation (Bergan & Knarud, 1993; Ryseth, 2014). The dramatic maturity contrast in the southern SWBSB was also documented by Mørk (1999) and Fleming et al. (2016), who linked sandstone maturity to a predominance of Caledonian and Fennoscandian zircon age signatures. The present study records similar findings from the southern basin margin, where detrital zircon age data link clean quartz arenites of the Norian Fruholmen Formation to an abundance of Fennoscandian zircon ages and an absence of age populations younger than 350 Ma. Strong compositional contrast

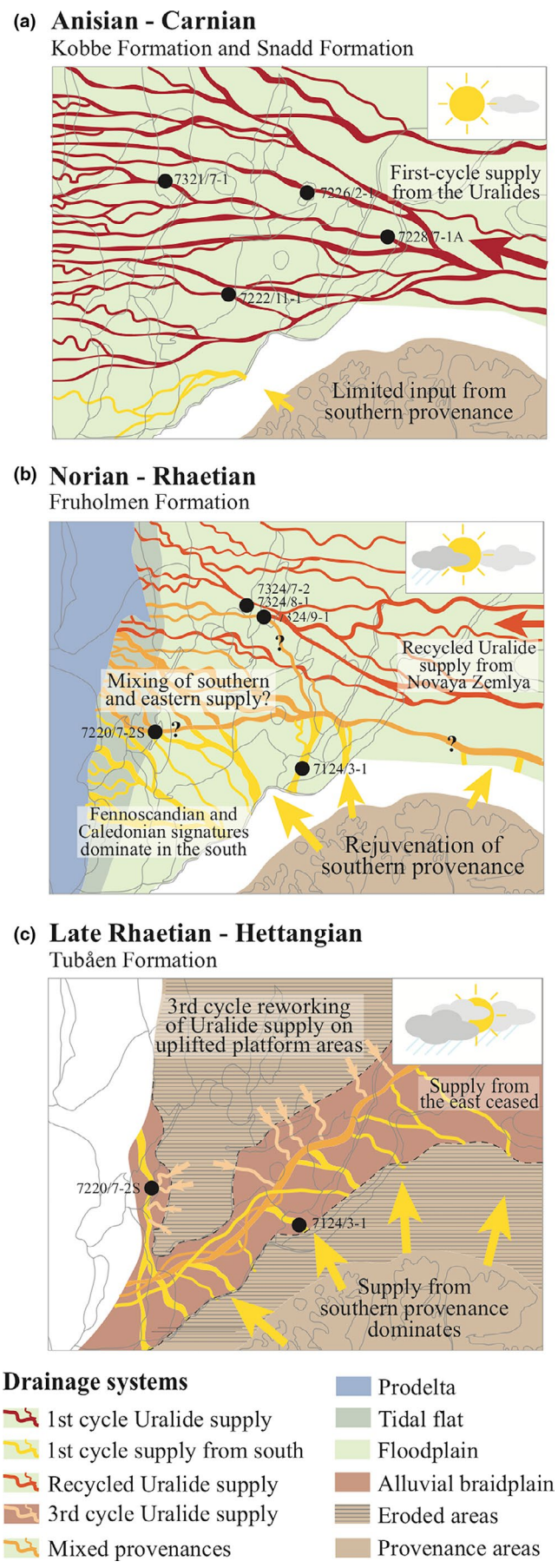

FIGURE 8 Conceptual paleogeographic maps of the southwestern Barents Sea basin show the interpreted regional development of sediment dispersal patterns from Anisian–Carnian (a) to Norian–Rhaetian (b) and Late Rhaetian–Hettangian (c)

with the immature, Uralide-sourced Snadd Formation below suggests that the maturity increase along the southern basin margins arise from a shift in provenance. Petrographic and geochronological data may thus indicate that the hinterland rejuvenation in the south started to influence sediment dispersal patterns along the southern basin margin in the Norian, or simply that the southern provenance continuously contributed with sediments to the southern part of the basin since the Early Triassic (Eide et al., 2017).

Subtle petrographic variations between the Fruholmen Formation and older Triassic sandstones from the basin interior (Haile et al., 2018; Line et al., 2018) suggest that strong compositional maturity contrasts across the Early Norian flooding surface can be associated with proximity to the rejuvenated hinterland in the south. The long-lived misconception of a distinct, regional compositional contrast in the Arctic at the turn of the Norian can be attributed to higher sampling frequency along the southern basin margins and camouflaging by subsequent maturation processes, such as increased annual precipitation and reworking.

The presence of a pronounced Timanide age peak in the zircon data from the Mercurius High, and a less prominent Caledonian peak in the Hoop area, indicates that sediment routing systems also existed between the southern hinterlands and the northern basin interior during the Norian (indicated in orange, Figure 8b). However, because geochronological data from the basin interior generally indicate minor supply from the southern provenance regions, petrographic signatures from other source terrains would be less obscured by quartz-rich sediment supply from the rejuvenated hinterland.

At first, abundant Uralide-aged zircon grains in the Fruholmen Formation from the basin interior appear to represent continued sedimentation from the southeast after the Early Norian transgression. However, fluid inclusion measurements conducted on Norian sandstones from the basin interior and the Svalbard archipelagos attest to burial temperatures of 130°C, which significantly depart from the normal burial history of the western Barents shelf (Haile et al., 2018). Parts of the Fruholmen Formation grain assembly can therefore unequivocally be attributed to recycling of a deeply buried and consolidated sedimentary basin. The absence of such abnormal temperatures in underlying Triassic formations suggests that the recycled particles were introduced to the western Barents Sea basin after the Early Norian.

The first appearance of recycled quartz grains coincides with a redistribution of chlorite at the Carnian–Norian transition. Predominantly distributed as grain coatings in the Snadd

and Kobbe formations (Line et al., 2018), chlorite is mainly recorded as pore-fill in the Fruholmen Formation from the present study. This rearrangement of ferric clay material further substantiates a recycled origin for the Fruholmen Formation sandstones in the basin interior.

Recycled sedimentary detritus in the Fruholmen Formation from the basin interior must either have been sourced locally from uplifted parts of the Barents shelf, as proposed by Fleming et al. (2016), or from an exposed hinterland that formed a sedimentary basin prior to substantial uplift (Klausen et al., 2017; Müller et al., 2019). Because the size and denudation profiles of local catchments cannot explain the high-temperature signatures and regional dispersal of the recycled detritus, the provenance should comprise a significantly larger area, where deeply buried sediments have been uplifted and exposed. As the closest tectonically active region at the time, the Novaya Zemlya fold-and-thrust belt represents the best provenance candidate for recycled Norian–Rhaetian detritus in the basin interior (indicated in bright red, Figure 8b). The Triassic succession deposited while the Novaya Zemlya area formed a basin at the northern edge of the Polar Uralides can likely account for the Uralide-aged zircons recorded in recycled Norian–Rhaetian sandstones from the basin interior. A recycled Uralide-origin also reconciles with the mineralogical similarities between the Fruholmen Formation and older Triassic strata. However, mixing of first-cycle detritus from the Polar Uralides and recycled detritus from exposed strata on Novaya Zemlya cannot be excluded from the present study.

The influx of zircon grains younger than 220 Ma (Figure 7h') affirms that an igneous provenance area was active while, or shortly before, supplying sediment to the SWBSB in the Norian (Klausen et al., 2017). The close match between the youngest zircon ages and depositional age implies that the igneous provenance was situated within geographical proximity to the western Barents shelf at the time of deposition. Igneous activity associated with the tectonically active fold-and-thrust belt to the east could explain the progressive younging of Late Triassic grains in stratigraphically younger sections, although this interpretation remains speculative in the absence of confidently documented Triassic granitic magmatism on Novaya Zemlya (Lopatin, Pavlov, Orgo, & Shkarubo, 2001). Eolian transport of young zircon grains can be excluded based on the occurrence of Jurassic age peaks in coeval strata from the Russian Barents Sea sector, and the absence of similar ages in contemporaneous strata from the SWBSB (Klausen et al., 2017). Based on the recorded occurrences of coeval zircon and depositional ages, Klausen et al. (2017) postulated that sedimentation from the igneous provenance to the basin interior culminated in the Sinemurian.

It is significant that the young (<220 Ma) zircon grains recorded in the Barents Sea closely match maximum depositional age in the basin interior throughout the Late Triassic, until basin inversion at the Jurassic–Triassic boundary. A more precise dating of the youngest grains could be achieved through application of CA-TIMS or multiple LA-ICP-MS analysis (Herriot, Crowley, Schmitz, Wartes, & Gillis, 2019), but this is beyond the scope of the present study. However, SEM of analysed grains indicates no structural damage that would suggest lead loss. Although the possibility of lead loss cannot be discounted, we emphasise that the age of analysed zircon grains rarely falls significantly below maximum depositional age of Late Triassic deposits in either Triassic or Jurassic samples. Consequently, potential lead loss would be highly coincidental with this persistent age signature.

Although the first signatures from the southern hinterland rejuvenation are registered already in the Norian, the transition from floodplain, tidal flat and fluvial environments into alluvial braidplain facies at the Fruholmen–Tubåen boundary (Figure 2a,b) is interpreted as the main phase of tectonic activity along the southern basin margins. The Latest Rhaetian–Hettangian Tubåen Formation was deposited in a narrow SW-NE oriented basin, delineated by the rejuvenated hinterland in the south and exposed platform areas to the north (Figure 8c). Hinterland rejuvenation combined with decreased subsidence rates in the Early Jurassic likely facilitated supply and preservation of medium- to coarse-grained deposits in the basin (Ryseth, 2014). Zircon spectra from the southern basin margin support continued sedimentation from the Baltic shield, thereby linking coarser particles to the southern provenance. On the remaining platform areas, the absence of the Rhaetian–Sinemurian succession represents a period of subaerial exposure and erosion of underlying Triassic strata (Klausen, Müller, Poyatos-Moré, Olaussen, & Stueland, 2019; Müller et al., 2019).

In the western basin interior, the two distinct grain size populations (Figure 4d) are interpreted to represent a combination of first-cycle supply from the south (indicated in yellow, Figure 8c) and recycled sediment from exposed platform areas in the basin interior (indicated in beige, Figure 8c). The combination of a subtle age peak from the Caledonian orogen and a Late Carboniferous age peak attests to a mix of bedrock lithologies in the southern provenance area. Although Carboniferous ages are common in the detrital zircon samples (related to rifting in the Barents Sea, volcanism in the Sverdrup Basin; Faleide, Gudlaugsson, & Jacquart, 1984, or the orogeny in the Uralides; Puchkov, 2009), it is rare to see a solitary peak of this age such as in the Tubåen Formation from the western basin interior (Figure 7d). This can be caused by sampling bias, or local variations in sediment supply, but the apparent absence of Triassic ages suggest it is derived locally rather than from the Uralides, where mixing with younger ages is common. Thus, our results imply that sedimentation from the east might have ceased in the western basin interior by the Hettangian.

As the Norian–Rhaetian succession in the basin interior is interpreted as recycled detritus from exposed strata in the Novaya Zemlya hinterland, it follows that local erosion of uplifted strata on platform areas during the Hettangian represents a second reworking cycle of Uralide-sourced sediment. In addition, textural and mineralogical properties might be modified a third time in the depositional environment. However, because braidplain deposits normally are associated with poor sorting parameters, we attribute the extreme compositional maturity in the Tubåen Formation from the basin interior to multiple cycles of reworking in combination with mature, first-cycle supply from the south.

5.2 | Temporal climatic variations

Discrepancies in the feldspar and clay contents between the Fruholmen Formation and the Kobbe and Snadd formations in the basin interior suggest that higher annual precipitation established after the Carnian (Figure 9). An average drop of 10% in total feldspar content coincides with a similar increase in kaolin, indicating a shift towards higher diagenetic weathering from Carnian to Norian. These observations are in line with palynological records in the Nordkapp Basin that reflect an increase in humidity towards the end of the Carnian (Hochuli & Vigran, 2010). A similar climatic trend was reported from east Greenland, where an increase in the kaolinite/illite ratio is recognized through the Late Triassic to the Early Jurassic succession (Decou, Andrews, Alderton, & Morton, 2017). Müller (2003) also recognized a long-term shift from arid/semi-arid to humid climate conditions in the northern North Sea region during the Rhaetian to Early Jurassic. In contrast to neighbouring shelves in the south and west, climate-enhanced mineralogical maturation in the Barents Sea has likely been obscured by contemporaneous quartz enrichment from provenance shifts and recycling.

Arrows in Figure 9 indicate a gradual increase in the kaolin content towards the top of the cored Fruholmen Formation at several basin locations. This kaolin profile is best developed in the upper Fruholmen Formation from the western basin interior, where the kaolin content increases from <5% to 20% over a 20-m interval (Figure 3f). Also, kaolin portions double over a 6-m section representing the N2 petrographic assembly from the northern basin interior (Figure 5f). Along the southern basin margins, an absence of kaolin in the medium-grained Fruholmen Formation is replaced by >20% kaolin over a 14-m interval (Figures 3c and 4b). The lack of a gradual trend in the southern core is likely related to lower sampling frequency. As wetter climatic conditions were already established after the Carnian, the kaolin increase towards the T–J boundary can either reflect enhanced leaching capacity or a further increase in annual precipitation towards the end of the Triassic. The profile's occurrence directly below an erosive, regional sequence boundary might suggest that subaerial exposure facilitated meteoric leaching of permeable, underlying strata. This process could link kaolin profiles in the basin interior to compression-induced uplift associated with the Novaya Zemlya protrusion in the east, and the development of a forebulge on the western Barents shelf (Müller et al., 2019). A similar explanation could be used for the extreme kaolin content in the upper Fruholmen Formation from the southern basin margin, where the uplift would be associated with the rejuvenation of the southern hinterlands. However, as this interpretation assumes that the kaolin material is the product of intensified leaching of feldspars and micas, the significant increase in kaolin (up to 20%) should be coupled with an equal decrease in feldspar and mica contents. This relationship has not been confirmed from the present study. Leaching below the sequence boundary would also imply that characteristic kaolin booklets should dominate the intergranular pore space. Although in-situ booklets are recorded, the significant kaolin increase is attributed to an abundance of small, anhedral kaolin crystals that occur in a mixed assembly with other clay fraction particles (Figure 4e). Based on the morphology and mixed composition of the pore-fill, we consider it more likely that an influx of allogenic kaolin accounts for the significant increase. Aluminium-rich clay particles are interpreted as the remnants of floodplain clays that were incorporated into channelized sandstones during fluvial erosion and river bank collapse. Because this interpreted origin implies that aluminium-rich soil profiles were already developed on the floodplain prior to incorporation in the channels, elevated kaolin contents in the upper Fruholmen Formation are attributed to higher annual precipitation in the latest Triassic. The regional distribution of the kaolin profiles also supports a climatic origin. Subsequent erosion and reworking have likely resulted in partial preservation of the kaolin profiles in the SWBSB, thus explaining their absence in Norian sandstones from the Hoop Fault Complex. Nonetheless, further analyses targeting the pore-filling kaolin material are necessary to investigate a potential relation to the T–J sequence boundary.

FIGURE 9 A significant kaolin increase occurs towards the T–J boundary in all studied cores (indicated by arrows). The marked drop in feldspars and kaolin across the T–J boundary, coupled with continuous Triassic age peaks, indicate reworking of Uralide-sourced particles until the Aalenian. XRD data from the Kobbe and Snadd formations were retrieved from Line et al. (2018)

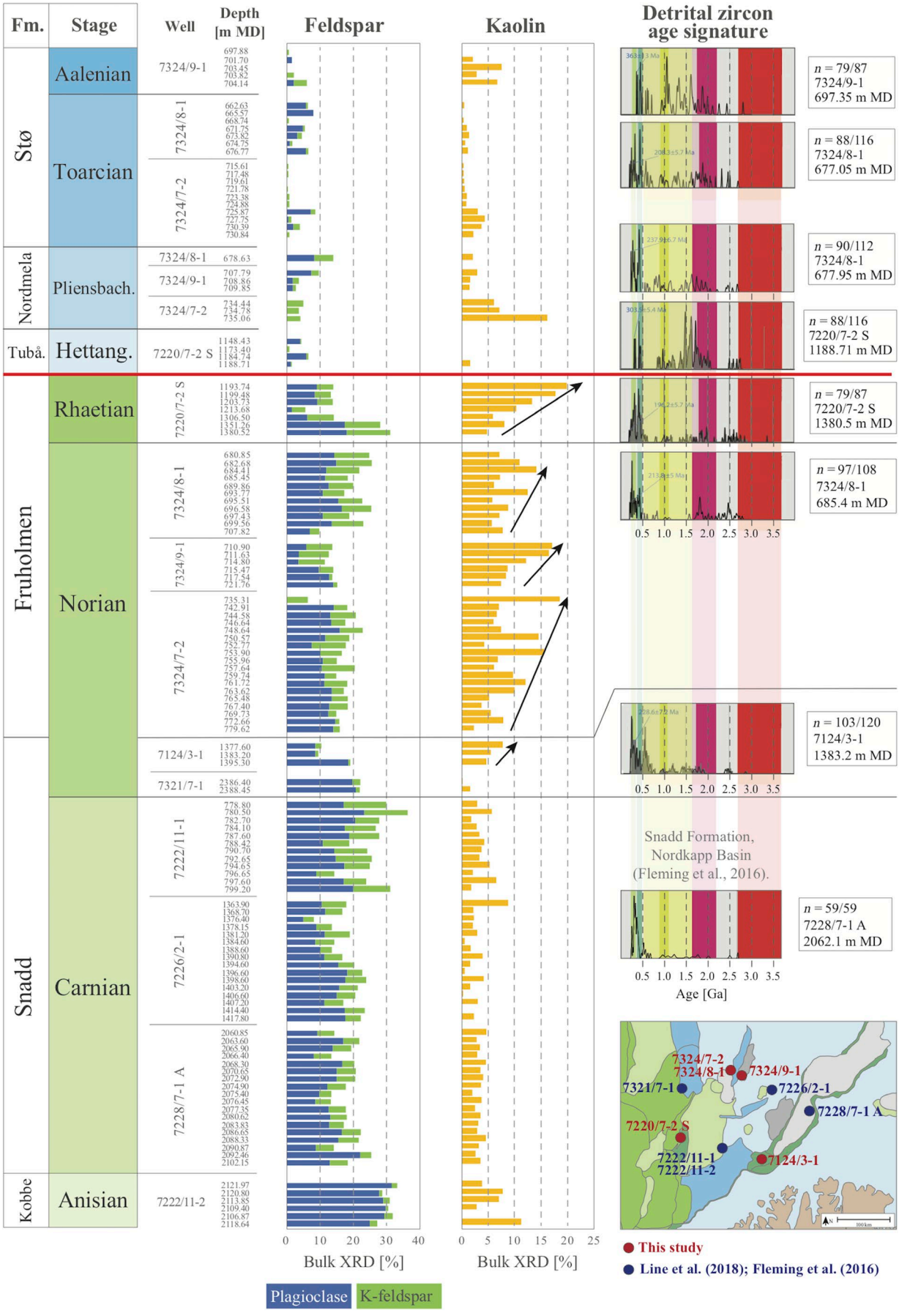
Fm.
Stage
Well
Depth [m MD]
Feldspar
Kaolin
Detrital zircon age signature
Stø
Aalenian
Toarcian
Nordmela
Pliensbach.
Tubå.
Hettang.
Fruholmen
Rhaetian
Norian
Snadd
Carnian
Kobbe
Anisian
7324/9-1
7324/8-1
7324/7-2
7220/7-2 S
7124/3-1
7321/7-1
7222/11-1
7226/2-1
7228/7-1 A
7222/11-2
n = 79/87
7324/9-1
697.35 m MD
n = 88/116
7324/8-1
677.05 m MD
n = 90/112
7324/8-1
677.95 m MD
n = 88/116
7220/7-2 S
1188.71 m MD
n = 79/87
7220/7-2 S
1380.5 m MD
n = 97/108
7324/8-1
685.4 m MD
n = 103/120
7124/3-1
1383.2 m MD
Snadd Formation,
Nordkapp Basin
(Fleming et al., 2016).
n = 59/59
7228/7-1 A
2062.1 m MD
0.5 1.0 1.5 2.0 2.5 3.0 3.5
Age [Ga]
0 10 20 30 40
Bulk XRD [%]
0 5 10 15 20 25
Bulk XRD [%]
Plagioclase
K-feldspar
This study
Line et al. (2018); Fleming et al. (2016)

5.3 | Sediment recycling at the Triassic–Jurassic transition

Two distinct recycling processes are recognized across the Triassic–Jurassic transition in the SWBSB: (a) Recycling of a deeply buried sedimentary basin in the hinterland and (b) local erosion of exposed intrabasinal highs and platform areas in the western Barents shelf. In addition, it is likely that textural and mineralogical modification of sediments in marginal-marine depositional environments have contributed to mechanical breakdown of labile components and particle rounding in the Jurassic. In this section, we discuss recycling signatures recorded in the Fruholmen, Tubåen, Nordmela and Stø formations by comparing textural properties above and below the T–J boundary at the various basin locations (Figure 10).

This study documents intra-formational petrographic variations within the Fruholmen Formation in the basin interior. The western and N2 mineral assemblies are more quartz-rich compared to the northern sandstone assembly and contains six times the average percentage of rounded grains (compare Figure 10a,c). Although textural maturity might be related to tidal influence (Figure 2b,d), a facies-dependent relationship alone cannot explain the absence of ferric minerals in the western and N2 assemblies. As large parts of the Norian–Rhaetian succession are missing across the northern basin interior due to subaerial exposure and denudation (Klausen et al., 2019), upper sections of the Fruholmen Formation in the western basin interior could contain recycled detritus from exposed strata on northern platform areas. A recycled origin could also account for the portion of Triassic zircons in the western petrographic assembly (Figure 7e). However, as the Caledonian age signature is more pronounced in the west, and mature petrographic properties occur on the northern platform, we consider supply from the south as a more likely explanation for higher compositional maturity in the western and N2 assemblies. Also, the presence of contemporaneous zircon grains (<200 Ma) does not reconcile with a reworking scenario for the Fruholmen Formation in the west, and rather suggests a supply of first-cycle sediments in the Latest Triassic. Thus, the ambiguous signatures of the western and N2 sandstone suites in the Fruholmen Formation could be indicative of a mixed and/or recycled origin. Although the mechanisms behind the intra-formational variations within the Fruholmen Formation in the basin interior are poorly understood, their existence documents a potential for preserving texturally and mineralogically mature sandstones with Uralide age signatures.

As parts of the Fruholmen Formation in the basin interior are interpreted as recycled detritus from an uplifted sedimentary basin in the hinterland (Novaya Zemlya), it follows

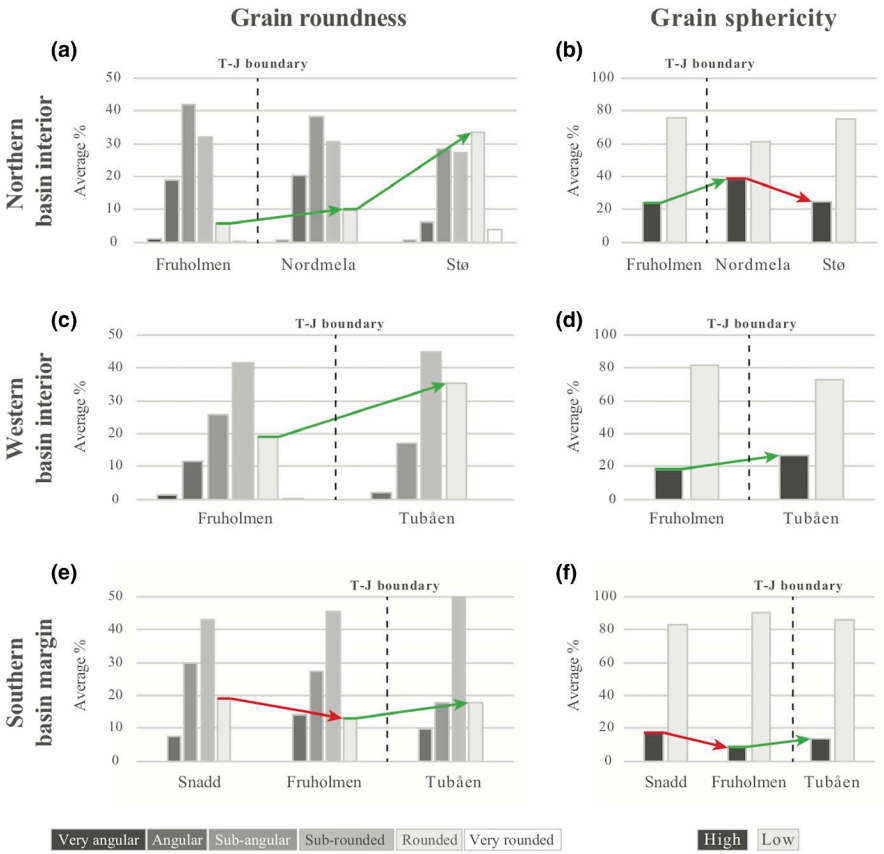

FIGURE 10 Average grain roundness and sphericity in the Upper Triassic–Middle Jurassic succession show higher textural maturity above the Triassic–Jurassic (T–J) boundary in the basin interior (a–d). By comparison, the textural maturity increase from the Fruholmen Formation to the Tubåen Formation along the southern basin margin is subtle (e and f). Arrows indicate increasing (green) and decreasing (red) portions of rounded and high sphericity grains that are used as a proxy for textural maturity

that subsequent local erosion of uplifted platform areas in the earliest Jurassic represents a second reworking cycle of sediments originally sourced from the Uralides. Multiple cycles of reworking, in addition to quartz-rich supply from the rejuvenated hinterland in the south, can therefore explain the extreme compositional maturity registered in the Tubåen Formation. High textural maturity supports a local reworking scenario in the western basin interior (Figure 10c–d), whereas the lower textural maturity in the Fennoscandia-derived Tubåen Formation along the southern basin margin (Figure 10d–f) likely reflects a short source-to-sink profile and limited reworking in the braidplain environment.

The Pliensbachian Nordmela Formation in the northern basin interior displays similar zircon age spectra as the Fruholmen Formation below, indicating that a portion of the detritus might represent particles originally derived from the Uralide Orogeny (Figure 7g,j). The mineralogical maturity that distinguishes the Nordmela Formation from the formations below the 20-million-year long hiatus (Figure 5f) can likely be attributed to the signatures from the southern provenance. The absence of contemporaneous zircon grains in the Nordmela Formation might imply that supply from the active igneous source to the western Barents shelf had terminated before the Pliensbachian. Using the minimum zircon age peaks as a proxy for sedimentation from the east, Klausen et al. (2017) related the absence of these grains to the development of a foredeep basin west of the Novaya Zemlya fold-and-thrust belt. It has been postulated that the foredeep basin, combined with elevated sea level, shielded the western Barents shelf from eastern sediment supply after the Sinemurian (Klausen et al., 2017; Sømme, Doré, Lundin, & Tørudbakken, 2018). Following this interpretation, Triassic age peaks recorded in the Nordmela Formation from the SWBSB represent recycled components sourced locally from inside the basin. An intrabasinal origin for the Nordmela Formation, combined with local reworking in tidal to shallow marine environments, is supported by the high textural maturity documented across the T–J boundary in the northern basin interior (Figure 10a–b) and underscores how important multiple episodes of reworking is for reservoir quality.

The textural maturation trend across the T–J boundary continues into the Toarcian–Aalenian Stø Formation, where most grains are rounded (Figure 10a). Geochronological zircon data suggest that sediment supply from the south became increasingly more important stratigraphically upward in the basin interior since the Pliensbachian (Figure 7f,i). Although the abundance of rounded grains might insinuate pronounced recycling of particles comprising the Stø Formation, first-generation supply from the southern provenance is likely obscured in this plot because coarser particles are more readily rounded than fine-grained sand due to their smaller surface area. Significant depositional hiatuses are typical of the Early-Middle Jurassic succession in the SWBSB, and condensed deposits might hold reworked constituents from the eroded time spans. An example from this study is the concentrically laminated pyrite grains recorded from the Stø Formation (Figure 6e), which have been interpreted as the remnants of ooidal grains that could have formed in a shallow marine setting dominated by bidirectional currents. Detailed analyses of condensed and transgressive lag deposits from the Early-Middle Jurassic succession may disclose depositional and climatic conditions prior to erosion, thereby allowing for a more complete understanding of the Early-Middle Jurassic period.

5.4 | General implications

The Triassic–Jurassic succession in the Barents Sea Basin documents a passage from a high-accommodation basin where predominantly immature sandstone compositions were deposited, to a low-accommodation basin characterized by sediment starvation and bypass. As a consequence of the structural reorganization in the basin and of the surrounding hinterland terrains, a gradual shift towards higher compositional and textural maturity have enhanced the reservoir quality of siliciclastic sandstones over time. Such transitions have crucial implications for petroleum exploration and development strategies for the studied succession but also for other sedimentary basins of equivalent tectonic setting. Thus, understanding regional and local processes contributing to textural and mineralogical maturation of siliciclastic sediment over time is important.

The Lower-Middle Mesozoic succession in the Barents Sea provides an excellent example of the influence provenance shifts, climatic changes, diagenesis, sedimentary facies and recycling have on modifying siliciclastic sediment towards higher mineralogical and textural maturity. However, unravelling the effects of these interrelated processes on compositional maturation from the stratigraphic record can be challenging. This study demonstrates that compositional changes associated with provenance shifts can be distinguished from processes related to climatic changes, diagenesis and sedimentary facies by integrating mineralogical and textural analyses with geochronological zircon data. Also, sediment recycling has proven to be difficult to decipher solely using geochronology, and validation relies on complementing it with mineralogical analyses and high-resolution petrographic methods.

6 | CONCLUSION

This study documents geographical and temporal variations in sediment composition and dispersal patterns across the

Triassic–Jurassic boundary in the SWBSB. Compositional and textural maturity of sandstone reservoirs vary with basin location and appear to increase gradually from the Late Carnian–Early Norian to the Middle Jurassic.

Rejuvenation of the Caledonian and Fennoscandian hinterlands in the Early Norian facilitated influx of coarser and quartz-rich sedimentary particles, which produced a strong contrast to the underlying, fine-grained lithic arkoses and litharenithic detritus that had dominated the basin since the Early Triassic. Our study indicates that previously recorded petrographic contrasts across the Early Norian flooding surface in the southern basin margin arise from a local shift in provenance. The long-lived misconception of a regional compositional contrast in the Arctic at the turn of the Norian can be attributed to higher sampling frequency associated with hydrocarbon exploration activity along the southern basin margins, and camouflaging by subsequent sediment modification processes, such as increased annual precipitation and reworking.

New data from the basin interior reveal a more subtle compositional maturity increase from the Carnian to the Norian, which we attribute to recycling of older Triassic strata deposited in a deep sedimentary basin. The uplifted Novaya Zemlya fold-and-thrust belt represents the best provenance candidate for recycled components in Norian–Rhaetian sandstones from the basin interior. Higher annual precipitation after the latest Carnian likely amplified mineralogical maturation of sandstones across the Triassic–Jurassic boundary, but we consider the effect of climatic weathering as inferior to other maturation processes, such as provenance shifts and reworking. Intra-formational variations within the Fruholmen Formation in the basin interior might be attributed to reworking of uplifted strata on platform areas, but ambiguous signatures of the preserved succession in the west are indicative of a mixed origin that require further analyses.

We recognize at least two sources for recycled grains from the Upper Triassic–Middle Jurassic succession in the SWBSB. The first represents the recycling of a deep sedimentary basin in the hinterland, where sediments with high-temperature signatures, Triassic and contemporaneous zircon ages are supplied to the western Barents shelf during the Norian–Rhaetian.

A subsequent, and possibly overlapping, phase of local reworking in the SWBSB is inferred from pronounced truncation of Upper Triassic strata in the basin interior. Both recycling episodes can likely be attributed to compression induced by the Novaya Zemlya fold-and-thrust belt, where recycled grains were shed westward from the uplifted hinterland and later redistributed during forebulge uplift in the Jurassic.

A third probable sediment modification scenario follows sea level fluctuations and corresponding depositional facies, where shallow marine conditions and multiple transgressions in the Jurassic likely facilitated textural maturation of condensed sections. The development of a foredeep basin west of the Novaya Zemlya fold-and-thrust belt in the Sinemurian–Pliensbachian is thought to have shielded the western Barents shelf from eastern sediment supply, after which intrabasinal sedimentation commenced in the basin interior.

In addition to increased supply from the rejuvenated hinterland in the south, the accumulation of polycyclic grains stratigraphically upwards can explain the extreme compositional maturity registered in the Tubåen, Nordmela and Stø formations in the SWBSB.

ACKNOWLEDGEMENTS

The principal author is funded by VISTA (project 6270) – a basic research collaboration programme between the Norwegian Academy of Science and Letters, and Equinor (former Statoil). We also wish to thank our project sponsor OMV Norge, particularly Eirik Stueland, for funding and access to core data from the Hoop area. A. F. Clark, T. G. Ilagan and J. Lindtorp are thanked for their efforts in sample preparation and microscopy analyses. Detrital zircon analyses were performed at the University of Bergen, and we are thankful for laboratory assistance from S. Hjort Dundas, I. Dumitru, M. Suppersberger and L. E. Rydland Pedersen. B. G. Haile provided useful comments while reviewing the manuscript. The data that support the findings of this study are provided in the supplementary material.

DATA AVAILABILITY STATEMENT

The data that support the findings of this study are available on request from the corresponding author. Geochronological zircon data and referenced core photos are available as supplementary material.

ORCID

Lina H. Line https://orcid.org/0000-0002-2352-5577

REFERENCES

Arctic Ocean relief location map.png. (2014, August 21). *Wikimedia Commons, the free media repository*. Retrieved from https://commons.wikimedia.org/w/index.php?title=File:Arctic_Ocean_relief_location_map.png&oldxml:id=132249753

Bergan, M., & Knarud, R. (1993). Apparent changes in clastic mineralogy of the Triassic–Jurassic succession, Norwegian Barents Sea: Possible implications for palaeodrainage and subsidence. *Norwegian Petroleum Society Special Publications*, *2*, 481–493. https://doi.org/10.1016/B978-0-444-88943-0.50034-4

Bue, E. P., & Andresen, A. (2014). Constraining depositional models in the Barents Sea region using detrital zircon U-Pb data from Mesozoic sediments in Svalbard. *Geological Society, London, Special Publications*, *386*(1), 261–279. https://doi.org/10.1144/SP386.14

Cohen, K. M., Harper, D. A. T., & Gibbard, P. L. (2018). ICS international chronostratigraphic chart 2018/08. *International Commission on Stratigraphy, IUGS*. Retrieved from www.stratigraphy.org (visited: 2018).

Decou, A., Andrews, S. D., Alderton, D. H., & Morton, A. (2017). Triassic to Early Jurassic climatic trends recorded in the Jameson Land Basin, East Greenland: Clay mineralogy, petrography and heavy mineralogy. *Basin Research*, *29*(5), 658–673. https://doi.org/10.1111/bre.12194

Dott, R. H. (1964). Wacke, graywacke and matrix; what approach to immature sandstone classification? *Journal of Sedimentary Research*, *34*(3), 625–632.

Eide, C. H., Howell, J. A., Buckley, S. J., Martinius, A. W., Oftedal, B. T., & Henstra, G. A. (2016). Facies model for a coarse-grained, tide-influenced delta: Gule Horn Formation (Early Jurassic), Jameson Land. *Greenland. Sedimentology*, *63*(6), 1474–1506. https://doi.org/10.1111/sed.12270

Eide, C. H., Klausen, T. G., Katkov, D., Suslova, A. A., & Helland-Hansen, W. (2017). Linking an Early Triassic delta to antecedent topography: Source-to-sink study of the southwestern Barents Sea margin. *GSA Bulletin*, *130*(1-2), 263–283. https://doi.org/10.1130/B31639.1

Faleide, J. I., Gudlaugsson, S. T., & Jacquart, G. (1984). Evolution of the western Barents Sea. *Marine and Petroleum Geology*, *1*(2), 123–150. https://doi.org/10.1016/0264-8172(84)90082-5

Faleide, J. I., Pease, V., Curtis, M., Klitzke, P., Minakov, A., Scheck-Wenderoth, M., … Zayonchek, A. (2018). Tectonic implications of the lithospheric structure across the Barents and Kara shelves. *Geological Society, London, Special Publications*, *460*(1), 285–314. https://doi.org/10.1144/SP460.18

Fleming, E. J., Flowerdew, M. J., Smyth, H. R., Scott, R. A., Morton, A. C., Omma, J. E., … Whitehouse, M. J. (2016). Provenance of Triassic sandstones on the southwest Barents Shelf and the implication for sediment dispersal patterns in northwest Pangaea. *Marine and Petroleum Geology*, *78*, 516–535. https://doi.org/10.1016/j.marpetgeo.2016.10.005

Flowerdew, M. J., Fleming, E. J., Morton, A. C., Frei, D., Chew, D. M., & Daly, J. S. (2019). Assessing mineral fertility and bias in sedimentary provenance studies: Examples from the Barents Shelf. *Geological Society, London, Special Publications*, *484*, SP484-11. https://doi.org/10.1144/SP484.11

Glørstad-Clark, E., Faleide, J. I., Lundschien, B. A., & Nystuen, J. P. (2010). Triassic seismic sequence stratigraphy and paleogeography of the western Barents Sea area. *Marine and Petroleum Geology*, *27*(7), 1448–1475. https://doi.org/10.1016/j.marpetgeo.2010.02.008

Gudlaugsson, S. T., Faleide, J. I., Johansen, S. E., & Breivik, A. J. (1998). Late Palaeozoic structural development of the south-western Barents Sea. *Marine and Petroleum Geology*, *15*(1), 73–102. https://doi.org/10.1016/S0264-8172(97)00048-2

Haile, B. G., Klausen, T. G., Czarniecka, U., Xi, K., Jahren, J., & Hellevang, H. (2018). How are diagenesis and reservoir quality linked to depositional facies? A deltaic succession, Edgeøya, Svalbard. *Marine and Petroleum Geology*, *92*, 519–546. https://doi.org/10.1016/j.marpetgeo.2017.11.019

Henriksen, E., Ryseth, A. E., Larssen, G. B., Heide, T., Rønning, K., Sollid, K., & Stoupakova, A. V. (2011). Tectonostratigraphy of the greater Barents Sea: Implications for petroleum systems. *Geological Society, London, Memoirs*, *35*(1), 163–195. https://doi.org/10.1144/M35.10

Herriott, T. M., Crowley, J. L., Schmitz, M. D., Wartes, M. A., & Gillis, R. J. (2019). Exploring the law of detrital zircon: LA-ICP-MS and CA-TIMS geochronology of Jurassic forearc strata, Cook Inlet, Alaska, USA. *Geology*, *47*(11), 1044–1048. https://doi.org/10.1130/G46312.1

Hochuli, P. A., & Vigran, J. O. (2010). Climate variations in the Boreal Triassic – Inferred from palynological records from the Barents Sea. *Palaeogeography, Palaeoclimatology, Palaeoecology*, *290*(1–4), 20–42. https://doi.org/10.1016/j.palaeo.2009.08.013

Klausen, T. G., Müller, R., Poyatos-Moré, M., Olaussen, S., & Stueland, E. (2019). Tectonic, provenance and sedimentological controls on reservoir characteristics in the Upper Triassic to Middle Jurassic Realgrunnen Subgroup-Southwest Barents Sea. *Geological Society, London, Special Publications*, *495*, SP495-2018. https://doi.org/10.1144/SP495-2018-165

Klausen, T. G., Müller, R., Slama, J., & Helland-Hansen, W. (2017). Evidence for Late Triassic provenance areas and Early Jurassic sediment supply turnover in the Barents Sea Basin of northern Pangea. *Lithosphere*, *9*(1), 14–28. https://doi.org/10.1130/L556.1

Klausen, T. G., Müller, R., Sláma, J., Olaussen, S., Rismyhr, B., & Helland-Hansen, W. (2018). Depositional history of a condensed shallow marine reservoir succession: Stratigraphy and detrital zircon geochronology of the Jurassic Stø Formation, Barents Sea. *Journal of the Geological Society*, *175*(1), 130–145.

Klausen, T. G., Ryseth, A. E., Helland-Hansen, W., Gawthorpe, R., & Laursen, I. (2014). Spatial and temporal changes in geometries of fluvial channel bodies from the Triassic Snadd Formation of offshore Norway. *Journal of Sedimentary Research*, *84*(7), 567–585. https://doi.org/10.2110/jsr.2014.47

Klausen, T. G., Ryseth, A. E., Helland-Hansen, W., Gawthorpe, R., & Laursen, I. (2015). Regional development and sequence stratigraphy of the Middle to Late Triassic Snadd formation, Norwegian Barents Sea. *Marine and Petroleum Geology*, *62*, 102–122. https://doi.org/10.1016/j.marpetgeo.2015.02.004

Line, L. H., Jahren, J., & Hellevang, H. (2018). Mechanical compaction in chlorite-coated sandstone reservoirs – Examples from Middle-Late Triassic channels in the southwestern Barents Sea. *Marine and Petroleum Geology*, *96*, 348–370. https://doi.org/10.1016/j.marpetgeo.2018.05.025

Lopatin, B. G., Pavlov, L. G., Orgo, V. V., & Shkarubo, S. I. (2001). Tectonic structure of Novaya Zemlya. *Polarforschung*, *69*, 131–135.

Ludwig, K. R. (2008). *Isoplot 3.70: A geochronological toolkit for Microsoft Excel* (Vol. *4*, p. 77). Berkeley, CA: Berkeley Geochronology Center, Special Publication.

Mangerud, G., & Rømuld, A. (1991). Spathian-Anisian (Triassic) palynology at the Svalis Dome, southwestern Barents Sea. *Review of Palaeobotany and Palynology*, *70*(3), 199–216. https://doi.org/10.1016/0034-6667(91)90002-K

Mørk, A., Knarud, R., & Worsley, D. (1982). Depositional and diagenetic environments of the Triassic and Lower Jurassic succession of Svalbard. *Arctic Geology and Geophysics: Proceedings of the Third International Symposium on Arctic Geology*, *8*, 371–398.

Mørk, M. B. E. (1999). Compositional variations and provenance of Triassic sandstones from the Barents Shelf. *Journal of Sedimentary Research*, *69*(3), 690–710. https://doi.org/10.2110/jsr.69.690

Müller, R. (2003). *Basin infill dynamics of the Triassic of the northern North Sea and Mid-Norwegian shelf: Control of autogenic and allogenic factors*. Doctoral dissertation. University of Oslo.

Müller, R., Klausen, T. G., Faleide, J. I., Olaussen, S., Eide, C. H., & Suslova, A. (2019). Linking regional unconformities in the Barents Sea to compression-induced forebulge uplift at the Triassic-Jurassic transition. *Tectonophysics*, *20*, 35–51. https://doi.org/10.1016/j.tecto.2019.04.006

Norwegian Petroleum Directorate. (2019, March 8).NPD factmaps. Retrieved from http://gis.npd.no/factmaps/html_21/

Powers, M. C. (1953). A new roundness scale for sedimentary particles. *Journal of Sedimentary Research*, *23*(2), 117–119. https://doi.org/10.1306/D4269567-2B26-11D7-8648000102C1865D

Puchkov, V. N. (2009). The evolution of the Uralian orogen. *Geological Society, London, Special Publications*, *327*(1), 161–195. https://doi.org/10.1144/SP327.9

Ryseth, A. (2014). Sedimentation at the Jurassic-Triassic boundary, south-west Barents Sea: Indication of climate change. *From Depositional Systems to Sedimentary Successions on the Norwegian Continental Margin*, *46*, 187–214.

Scotese, C. R. (2004). A continental drift flipbook. *The Journal of Geology*, *112*(6), 729–741. https://doi.org/10.1086/424867

Sømme, T. O., Doré, A. G., Lundin, E. R., & Tørudbakken, B. O. (2018). Triassic-Paleogene paleogeography of the Arctic: Implications for sediment routing and basin fill. *AAPG Bulletin*, *102*(12), 2481–2517. https://doi.org/10.1306/05111817254

Vigran, J. O. (2014). *Palynology and geology of the Triassic succession of Svalbard and the Barents Sea*. Norges Geologiske undersøkelse.

Wilson, M. D., & Pittman, E. D. (1977). Authigenic clays in sandstones; recognition and influence on reservoir properties and paleoenvironmental analysis. *Journal of Sedimentary Research*, *47*(1), 3–31.

Worsley, D. (2008). The post-Caledonian development of Svalbard and the western Barents Sea. *Polar Research*, *27*(3), 298–317. https://doi.org/10.1111/j.1751-8369.2008.00085.x

SUPPORTING INFORMATION

Additional supporting information may be found online in the Supporting Information section.

How to cite this article: Line LH, Müller R, Klausen TG, Jahren J, Hellevang H. Distinct petrographic responses to basin reorganization across the Triassic–Jurassic boundary in the southwestern Barents Sea. *Basin Res*. 2020;00:1–22. https://doi.org/10.1111/bre.12437